

Dalton Transactions

Accepted Manuscript



This is an *Accepted Manuscript*, which has been through the Royal Society of Chemistry peer review process and has been accepted for publication.

Accepted Manuscripts are published online shortly after acceptance, before technical editing, formatting and proof reading. Using this free service, authors can make their results available to the community, in citable form, before we publish the edited article. We will replace this *Accepted Manuscript* with the edited and formatted *Advance Article* as soon as it is available.

You can find more information about *Accepted Manuscripts* in the [Information for Authors](#).

Please note that technical editing may introduce minor changes to the text and/or graphics, which may alter content. The journal's standard [Terms & Conditions](#) and the [Ethical guidelines](#) still apply. In no event shall the Royal Society of Chemistry be held responsible for any errors or omissions in this *Accepted Manuscript* or any consequences arising from the use of any information it contains.

Oxidovanadium(IV) and dioxidovanadium(V) complexes of hydrazones of 2-benzoylpyridine and their catalytic applications

Mannar R. Maurya,*^a Nikita Chaudhary,^a Fernando Avecilla,^b Pedro Adão,^c and J. Costa Pessoa*^c

^a *Department of Chemistry, Indian Institute of Technology Roorkee, Roorkee-247667, India. E-mail: rkmanfcy@iitr.ernet.in; Fax: +91 1332 273560; Tel: +91 1332 285327*

^b *Departamento de Química Fundamental, Universidade da Coruña, Campus de A Zapateira, 15071 A Coruña, Spain*

^c *Centro de Química Estrutural, Instituto Superior Técnico, Universidade Lisboa, Lisboa 1049-001, Portugal. E-mail: joao.pessoa@ist.utl.pt; Fax: +351 21 8464455; Tel: +351 21 8419268*

((Abstract))

Reaction between the tridentate ONN donor ligands, Hbzpy-tch (**I**) and Hbzpy-inh (**II**) with $[V^{IV}O(acac)_2]$ in dry methanol gives two different types of complexes, $[V^{IV}O(acac)(bzpy-tch)]$ (**1**) and $[V^{IV}O(OMe)(bzpy-inh)]$ (**2**), respectively. Irrespective of their nature in methanol upon aerial oxidation and precipitation both yield dinuclear $[{V^V}O(bzpy-tch)]_2(\mu-O)_2$ (**3**) and $[{V^V}O(bzpy-inh)]_2(\mu-O)_2$ (**4**). Treatment of **1** or **2** in methanol with H_2O_2 yields the oxidomonoperoxidovanadium(V) complexes $[{V^V}O(bzpy-tch)]_2(\mu-O_2)_2$ (**5**) and $[V^VO(O_2)(bzpy-inh)]$ (**6**). Reaction of **3** and **4** with imidazolomethylpolystyrene cross-linked with 5% divinylbenzene (PS-im) in DMF give the polymer-supported PS-im $[V^VO_2(bzpy-inh)(MeOH)]$ (**7**) and PS-im $[V^VO_2(bzpy-tch)(MeOH)]$ (**8**). The compounds are characterized by various spectroscopic techniques and compounds **7** and **8** were also analyzed by thermal, atomic force microscopy (AFM), field-emission scanning electron micrographs (FE-SEM) as well as Energy dispersive X-ray (EDAX) studies. The molecular structures of **3-5** and of $[V^VO(O_2)(bzpy-inh)(H_2O)] \cdot 0.5MeOH$ (**6a**) were determined by single-crystal X-ray diffraction, confirming the μ -bis(O) and ONN binding mode in the dinuclear complexes **3** and **4**, as well as the side-on coordination of the peroxido ligand in **5** and **6a**. The polymer-grafted compounds **7** and **8** were used for the catalytic oxidation of isoeugenol using aqueous H_2O_2 as oxidant. The intermediate peroxido species, expected to be involved during catalytic action, were also generated from solutions of **1-4** and studied by UV-Vis and ^{51}V NMR. The catalytic activity of

the several systems was tested, the polymer-supported versions showing higher conversions than their neat counterparts. The polymer-supported complexes allow for recyclable catalytic systems, thus providing additional advantage over these homogeneous counterparts in terms of increased catalyst lifetime and easier separation from the reaction mixture.

Introduction

Trigonal bipyramidal $V^V O_2$ -complexes particularly with benzimidazole, imidazole, pyridyl and hydrazide derived monobasic tridentate ONN ligands have been considered as functional models of vanadium haloperoxidases (VHPOs), as such complexes can mimic oxidative halogenations and sulfoxidations, along with oxidation, by peroxide, of organic substrates.^{1,2,3,4} It has been frequently observed that interaction between monobasic tridentate ligands and $[V^{IV}O(acac)_2]$ under aerobic conditions produces dinuclear, pseudo-octahedral complexes with the $[(V^V O)_2(\mu-O)_2]$ core unless bulky groups are attached to the ligand to provide sufficient steric hindrance.^{5,6} We observed that such condition is not necessary and even $V^V O_2$ -complexes of ligands having less steric hindrance can be crystallized in monomeric as well as dinuclear forms in different solvent systems.³ However, they are expected to exist in the mononuclear form in coordinating solvents.^{3a,3c} Our work in this direction led us to design monobasic tridentate ONN donor ligands having bulky groups (Scheme 1), to prepare the respective V^V -compounds and verify whether mononuclear $V^V O_2$ - or dinuclear $[(V^V O)_2(\mu-O)_2]$ -type complexes are obtained.

We observed that trigonal bipyramidal $V^V O_2$ -complexes can expand their coordination sphere and bind covalently with the nitrogen atom of the imidazole functionalized chloromethylated polystyrene, cross-linked with 5 % divinylbenzene.^{3b,3c,7} Such method of immobilizing e.g. molybdenum complexes has also been reported by others.⁸ This method is quite simple compared to methods where available linkages such as carboxylate, hydroxyl, sulphonate, imine etc. must be present in the ligand sphere of the metal to allow immobilization on e.g. chloromethylated polystyrene.^{9,10}

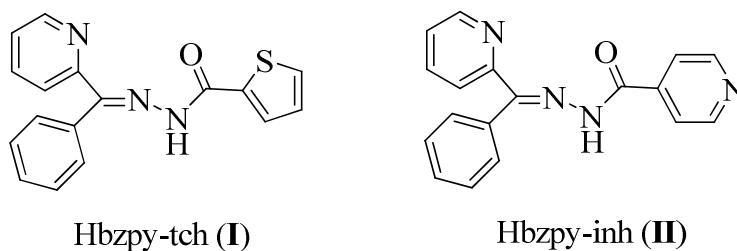
The developments of immobilized polymer vanadium complexes have garnered considerable interest in recent years for catalytic oxidations and oxygen transfer reactions, including the oxidative halogenation of organic substrates.^{9,10} Such heterogeneous compounds allow for the development of environmentally benign catalytic systems in the sense that less

toxic solvents and terminal oxidants are used, and catalyst loss is minimized through recycling, and product separation methods may be simplified.^{9,10}

Continuing our efforts on exploiting the above method of immobilization, we also describe herein the synthesis of two polymer-supported V^V -complexes of ONN donor hydrazones of 2-benzoylpyridine via covalent bonding through imidazolomethylpolystyrene (cross-linked with 5 % divinylbenzene) (Scheme 1).

The V^V -polymer-supported compounds, as well as the corresponding neat analogues were used here for the oxidation of isoeugenol. Vanillin is a key compound in food industry to provide the characteristic aroma and flavor of vanilla bean. With an output of about 15,000 tons/year,¹¹ it is probably the second largest produced chemical aroma in the world.¹¹ Vanillin is mainly produced by the oxidation of isoeugenol, microbial biotransformation of isoeugenol having been the key method to produce vanillin and vanillic acid, and such application has been reported extensively in the literature;^{12,13} vanillic acid can be reduced to vanillin.¹⁴ Photocatalytic oxidation of isoeugenol over TiO_2 also produces vanillin.¹⁵ Catalytic transformation of isoeugenol to vanillin using Bu_4NVO_3 /pyrazine-2-carboxylic acid in the presence of H_2O_2 as oxidant was reported by Gusevskaya *et al.*¹⁶ Due to its commercial and industrial interest, research in this field to find more economically efficient processes for vanillin production is therefore of interest.

Intermediate peroxido species presumably involved during catalytic action were also isolated in the solid state as well as generated and characterized in solution. Related neat $V^V O_2$ -complexes derived from 2-benzoylpyridine have been reported by Kuriakose *et al.*, but no catalytic activities were reported for those systems.¹⁷



Scheme 1 Structural formulae of the ligands used in this study.

Experimental section

Materials and general methods

Analytical reagent grade V_2O_5 , thiophene-2-carboxylic acid hydrazide (Fluka Chemie, Switzerland), isonicotinic acid hydrazide, imidazole, (Loba Chemie, Mumbai, India), 2-benzoylpyridine, acetylacetone (Hacac) (Aldrich, U.S.A.), isoeugenol (S.D. Fine, India) and 30 % aqueous H_2O_2 were used as obtained. Samples of chloromethylated polystyrene [18.9 % Cl (5.35 mmol Cl per gram of resin)] cross-linked with 5 % divinylbenzene were offered by Thermax Limited, Pune, India. Other chemicals and solvents were of analytical reagent grade. Imidazolomethylpolystyrene (PS-im)^{7,8} $[V^{IV}O(acac)_2]$ ¹⁸ were prepared according to the reported methods.

Elemental analyses of the ligands and complexes were obtained with an Elementar model Vario-EL-III. Vanadium content in polymer-bound complexes was checked by Inductively Coupled Plasma spectrometry (ICP; Labtam 8440 plasma lab), as well as by TGA (see below). IR spectra were recorded as KBr pellets on a Nicolet NEXUS Aligent 1100 FT-IR spectrometer. Electronic spectra of the polymer-bound complexes were recorded in Nujol on a Shimadzu 1601 UV-Vis spectrophotometer by layering a mull of the sample on the inside of one of the cuvettes while keeping the other one layered with Nujol as reference. Spectra of non-polymer bound ligands and complexes were recorded in methanol. The EPR spectra were recorded either at room temperature or at 77 K (on glasses made by freezing solutions in liquid nitrogen) with a Bruker ESP 300E X-band spectrometer. 1H NMR spectra and ^{51}V NMR spectra were recorded on Bruker Avance II+ 300 MHz or 400 MHz spectrometers. 1H NMR spectra are referenced to the deuterated solvent shift. ^{51}V NMR spectra were recorded using a 4:1 mixture of DMF/acetone- d_6 as solvent and the δ (^{51}V) values are referenced relative to neat V^VOCl_3 . Thermogravimetric analyses of the complexes were carried out using Perkin Elmer (Pyris Diamond) under oxygen atmosphere. The micrographs and vanadium content of the polymer-anchored complexes were recorded on a FEI-Quanta 200 FEG field emission scanning electron microscope coupled with an energy dispersive X-ray analyses (EDAX) device. The samples were coated with a thin film of gold to prevent surface charging, to protect the surface material from thermal damage by the electron beam and to make the sample conductive. A Shimadzu 2010 plus gas-chromatograph fitted with a Rtx-1 capillary column (30 m \times 0.25 mm \times 0.25 μ m)

and a FID detector was used to analyze the reaction products and their quantifications were made on the basis of the relative peak area of the respective product. The identity of the products was confirmed using a GC-MS Perkin-Elmer, model Clarus 500 and comparing the fragments of each product with the library available.

Preparations

Preparation of ligands. Hbpy-tch I. This was prepared by adapting a procedure reported in the literature.¹⁹ A solution of 2-benzoylpyridine (0.915 g, 5.0 mmol) in methanol (15 mL) was added to a solution of thiophene-2-carboxylic acid hydrazide (0.710 g, 5.0 mmol) in methanol (10 mL) and the resulting reaction mixture was refluxed for 5 h on a water bath. After reducing the volume of the solution to ca. 5 mL, it was kept at room temperature, where a pale yellow solid separated out, which was then filtered off, washed with a small amount of methanol and dried in air. Yield: 85%. (Found: C, 66.2; H, 4.0; N, 13.5; S, 10.1%. Calcd for C₁₇H₁₃N₃OS (307.37): C, 66.42; H, 4.26; N, 13.67; S, 10.43 %).

Hbpy-inh II. This was prepared analogously to **I** considering 2-benzoylpyridine (0.915 g, 5.0 mmol) and isonicotinic acid hydrazide (0.685 g, 5.0 mmol) in methanol. Yield: 92%. Found: C, 72.0; H, 4.4; N, 14.2%. Calcd for C₁₈H₁₄N₄O (302.32): C, 71.50; H, 4.66; N, 14.0%.

Preparation of complexes. [V^{IV}O(acac)(bzpy-tch)] 1. A solution of Hbpy-tch (0.307 g, 1.0 mmol) in methanol (10 mL) was treated with [V^{IV}O(acac)₂] (0.265 g, 1.0 mmol) dissolved in methanol (10 mL) in one portion and the resulting reaction mixture was refluxed under stirring in an oil bath for 2 h. Upon reducing the solvent volume to ca. 10 mL and cooling to room temperature resulted in the precipitation of a green solid which was filtered off, washed with methanol and dried under *vacuum*. Yield: 87%. EPR (X-Band, DMF, 77 K): $g_z = 1.946$, $A_z = 167.3 \times 10^{-4} \text{ cm}^{-1}$; EPR (X-Band, CH₂Cl₂, 77 K): $g_z = 1.950$, $A_z = 167.5 \times 10^{-4} \text{ cm}^{-1}$. (Found: C, 55.4; H, 4.1; N, 9.1; S, 6.5%. Calcd for C₂₂H₁₉N₃O₄SV (472.41): C, 55.93; H, 4.05; N, 8.89; S, 6.78%).

[V^{IV}O(OMe)(bzpy-inh)] 2. Complex **2** was prepared analogously to **1**, replacing **I** by (bzpy-inh) (**II**). Yield: 85%. EPR (X-Band, DMF, 77 K): (primary species) $g_z^1 = 1.951$, $A_z^1 = 167 \times 10^{-4} \text{ cm}^{-1}$,

(secondary species) $A_z^2 = 159.4 \times 10^{-4} \text{ cm}^{-1}$. (Found: C, 57.4; H, 4.2; N, 14.2%. Calcd for $\text{C}_{19}\text{H}_{16}\text{N}_4\text{O}_3\text{V}$ (399.29): C, 57.15; H, 4.03; N, 14.03%).

[{V^VO(bzpy-tch)}₂(μ -O)₂] 3. Complex **1** (0.472 g, 1.0 mmol) was dissolved in hot methanol (100 mL) and air was passed through the solution with occasional shaking for 12 h. The color of the solution changed gradually from green to yellow. After reducing the volume to ca. 20 mL the solution was kept open for slow evaporation where the yellow solid of **3** was obtained within overnight. This was filtered and dried under *vacuum*. Yield: 84%. ⁵¹V NMR (400 MHz, DMF/acetone-d₆ 4:1, ppm): $\delta_V = -501$; (400 MHz, DMSO-d₆, ppm): $\delta_V = -502$. (Found: C, 52.5; H, 3.0; N, 10.7; S, 8.1%. Calcd for $\text{C}_{17}\text{H}_{12}\text{N}_3\text{O}_3\text{SV}$ (389.30): C, 52.44; H, 3.10; N, 10.79; S, 8.23%). Yellow crystals of **3** were grown by slow evaporation of its DMF solution in a week period time.

[{V^VO(bzpy-inh)}₂(μ -O)₂] 4. Compound **4** was prepared adopting the procedure described for **3** and replacing **1** by $[\text{VO}^{\text{IV}}(\text{OMe})(\text{bzpy-inh})]$ (**2**). This was filtered and dried under *vacuum*. Yield: 86%. ⁵¹V NMR (400 MHz, DMF : acetone-d₆ (4:1) or DMSO-d₆, ppm): $\delta_V = -502$. (Found: C, 56.0; H, 3.5; N, 14.4%. Calcd for $\text{C}_{18}\text{H}_{13}\text{N}_4\text{O}_3\text{V}$ (384.26): C, 56.26; H, 3.41; N, 14.58%). X-ray diffraction quality crystals for **4** were obtained by slow evaporation of its methanolic solution in air.

[{V^VO(bzpy-tch)}₂(μ -O₂)₂] 5. An aqueous 30% H₂O₂ (ca. 2 mL) was added drop wise to **3** (0.389 g, 0.50 mmol) dissolved in methanol (20 mL) with constant stirring at ambient temperature for 8 h. After reducing the solvent volume to ca. 10 mL it was kept for ca. 24 h where orange solid precipitated which was filtered off, washed with cold methanol (2 × 2 mL) and dried under *vacuum*. Yield: 70%. ⁵¹V NMR (400 MHz, DMF/acetone-d₆ 4:1, ppm): $\delta_V = -571$. (Found: C, 50.7; H, 2.9; N, 10.2; S, 8.2%. Calcd for $\text{C}_{17}\text{H}_{12}\text{N}_3\text{O}_4\text{SV}$ (405.30): C, 50.37; H, 2.98; N, 10.36; S, 7.91%). X-ray diffraction quality crystals for **5** were obtained by slow evaporation of its methanolic solution in air. No difference in IR of powder sample and crystals was observed.

[V^VO(O₂)(bzpy-inh)] 6. Compound **6** was prepared analogously to **5**, taking 0.5 mmol of **4**. This was filtered and dried under *vacuum* to give orange red powder. Yield: 62%. ⁵¹V NMR (400 MHz, DMF/acetone-d₆ 4:1, ppm): $\delta_V = -570$. (Found: C, 54.2; H, 3.2; N, 13.7%. Calcd for $\text{C}_{18}\text{H}_{13}\text{N}_4\text{O}_4\text{V}$ (400.26): C, 54.01; H, 3.27; N, 13.99 %). X-ray diffraction quality crystals of **6** having

formulation $[V^V O(O_2)(bzpy-inh)(H_2O)] \cdot 0.5MeOH$ (**6a**) were obtained by slow evaporation of its methanolic solution in air and picked up directly from the solution for X-ray analysis. IR spectrum of **6a** differs only slightly from **6**.

PS-im $[V^V O_2(bzpy-tch)]$ **7**. The polystyrene bound imidazole (PS-im, 1.0 g) was suspended in DMF (10 mL) for 2 h prior to the reaction. A solution of $[{V^V O(bzpy-tch)}_2(\mu-O)_2]$ (**3**) (1.56 g, 2.0 mmol) in DMF (20 mL) was then added to the above suspension of PS-im and the mixture was heated in an oil bath for 24 h at ca. 90 °C with gentle mechanical stirring. Then the polystyrene bound PS-im $[V^V O_2(bzpy-tch)]$ (**4**) was filtered and washed with DMF followed by hot methanol. It was dried at 120 °C in an air oven. Recovery yield: ca. 95%.

PS-im $[V^V O_2(bzpy-inh)]$ **8**. Complex **8** was prepared analogously to **7**, replacing **3** by **4** (1.54 g, 2.0 mmol). Recovery yield: ca. 90%.

X-Ray Crystal Structure Determination

Three-dimensional X-ray data were collected on a Bruker Kappa Apex CCD diffractometer at low temperature for **3**, **4**, **5** and **6a** by the ϕ - ω scan method. Reflections were measured from a hemisphere of data collected from frames, each of them covering 0.3° in ω . Of the 55659 for **3**, 60921 for **4**, 30202 for **5** and 34088 for **6a** reflections measured, all were corrected for Lorentz and polarization effects and for absorption by multi-scan methods based on symmetry-equivalent and repeated reflections, 5018, 2965, 2369 and 2188 respectively, independent reflections exceeded the significance level ($|F|/\sigma|F|$) > 4.0. Complex scattering factors were taken from the program package SHELXTL.²⁰ The structures were solved by direct methods and refined by full matrix least-squares on F^2 . In **3**, hydrogen atoms were located in the difference Fourier map and left to refine freely. In **4** and **5**, hydrogen atoms were included in calculated positions and refined in the riding mode. In **6a**, the hydrogen atoms were located in the difference Fourier map and left to refine freely, except for C(5), C(6), C(14) and C(16), which were included in calculated positions and refined in the riding mode. In **6a**, the hydrogen atoms of the water molecule were located in the difference Fourier map and fixed to oxygen atom. Refinements were done with allowance for thermal anisotropy of all non-hydrogen atoms. Further details of the crystal structure determinations are given in Table 1. A final difference Fourier map showed no residual density outside: 0.565 and -0.836 e.Å⁻³ for **3**, 2.055 and -0.709

$\text{e.}\text{\AA}^{-3}$ for **4**, 0.820 and $-0.853 \text{ e.}\text{\AA}^{-3}$ for **5** and 0.759 and $-0.594 \text{ e.}\text{\AA}^{-3}$ for **6a**. The highest residual density in **4** is $2.05 \text{ e.}\text{\AA}^{-3}$ at 0.02 \AA from V1. The weighting schemes were: $w = 1/[\sigma^2(F_o^2) + (0.081100 \text{ } P)^2 + 0.219200 P]$ for **3**, $w = 1/[\sigma^2(F_o^2) + (0.129400 \text{ } P)^2 + 0.908600 P]$ for **4**, $w = 1/[\sigma^2(F_o^2) + (0.079200 \text{ } P)^2 + 2.265900 P]$ for **5** and $w = 1/[\sigma^2(F_o^2) + (0.108700 \text{ } P)^2 + 0.000000 P]$ for **6a**, where $P = (|F_o|^2 + 2|F_c|^2)/3$, were used in the latter stages of refinement. The crystal of **5** presents important disorders on the phenyl and thiophene groups; these disorders were resolved and the atomic sites were observed and refined with anisotropic atomic displacement parameters. More specifically these disorders were refined using 162 restraints (SADI, SIMU, DELU and FLAT restraints were used). The site occupancy factors were 0.48745 for C(9A), C(10A), C(11A), C(12A) and C(13A) on the phenyl group and 0.51932 for S(1A) and C(5A) on the thiophene group. The thiophene group is a ring rotated by 180° . The chemical formula in **6a** correspond to a V-complex : methanol 1:0.5 stoichiometric moiety.

Table 1 Crystal data and structure refinement for $[\{\text{V}^{\text{V}}\text{O}(\text{bzpy-tch})\}_2(\mu\text{-O})_2]$ **3**, for $[\{\text{V}^{\text{V}}\text{O}(\text{bzpy-inh})\}_2(\mu\text{-O})_2]$ **4**, $[\{\text{V}^{\text{V}}\text{O}(\text{bzpy-tch})\}_2(\mu\text{-O}_2)_2]$ **5** and $[\text{V}^{\text{V}}\text{O}(\text{O}_2)(\text{bzpy-inh})(\text{H}_2\text{O})]\cdot 0.5\text{MeOH}$ **6a**

	3 (1018367)	4 (1018368)	5 (1018365)	6a (1018366)
Formula	$\text{C}_{17}\text{H}_{12}\text{N}_3\text{O}_3\text{SV}$	$\text{C}_{18}\text{H}_{13}\text{N}_4\text{O}_3\text{V}$	$\text{C}_{17}\text{H}_{12}\text{N}_3\text{O}_4\text{SV}$	$\text{C}_{18.5}\text{H}_{17}\text{N}_4\text{O}_{5.5}\text{V}$
Formula weight	389.30	384.26	405.30	434.30
T, K	100(2)	100(2)	100(2)	100(2)
Wavelength, \AA	0.71073	0.71073	0.71073	0.71073
Crystal system	Triclinic	Monoclinic	Monoclinic	Monoclinic
Space group	$P \bar{1}$	$P2_1/c$	$P2_1/c$	$P2_1/c$
$a/\text{\AA}$	8.3281(6)	14.6312(5)	10.2017(8)	10.2637(12)
$b/\text{\AA}$	9.6580(8)	8.2122(3)	10.1819(10)	22.806(3)
$c/\text{\AA}$	22.010(2)	14.4503(5)	16.4706(15)	8.1173(9)
α°	81.235(6)	90	90	90
β°	87.348(6)	110.765(2)	104.582(5)	105.364(7)
γ°	68.383(5)	90	90	90
$V/\text{\AA}^3$	1626.5(2)	1623.48(10)	1655.7(3)	1832.2(4)
Z	4	4	4	4
F_{000}	792	784	824	892
$D_{\text{calc}}/\text{g cm}^{-3}$	1.590	1.572	1.626	1.574
μ/mm^{-1}	0.760	0.638	0.755	0.585
θ ($^\circ$)	0.94 to 27.57	1.49 to 27.58	2.06 to 26.45	1.79 to 26.52
R_{int}	0.1076	0.0951	0.0774	0.1672
Crystal size/ mm^3	0.22 x 0.09 x 0.06	0.25 x 0.18 x 0.08	0.18 x 0.16 x 0.10	0.14 x 0.09 x 0.07

Goodness-of-fit on F^2	1.028	1.088	1.073	1.019
$R_1[I > 2\sigma(I)]^a$	0.0502	0.0698	0.0601	0.0652
wR_2 (all data) ^b	0.1530	0.2035	0.1682	0.2028
Largest differences peak and hole ($e\text{\AA}^{-3}$)	0.565 and -0.836	2.055 and -0.709	0.820 and -0.853	0.759 and -0.594

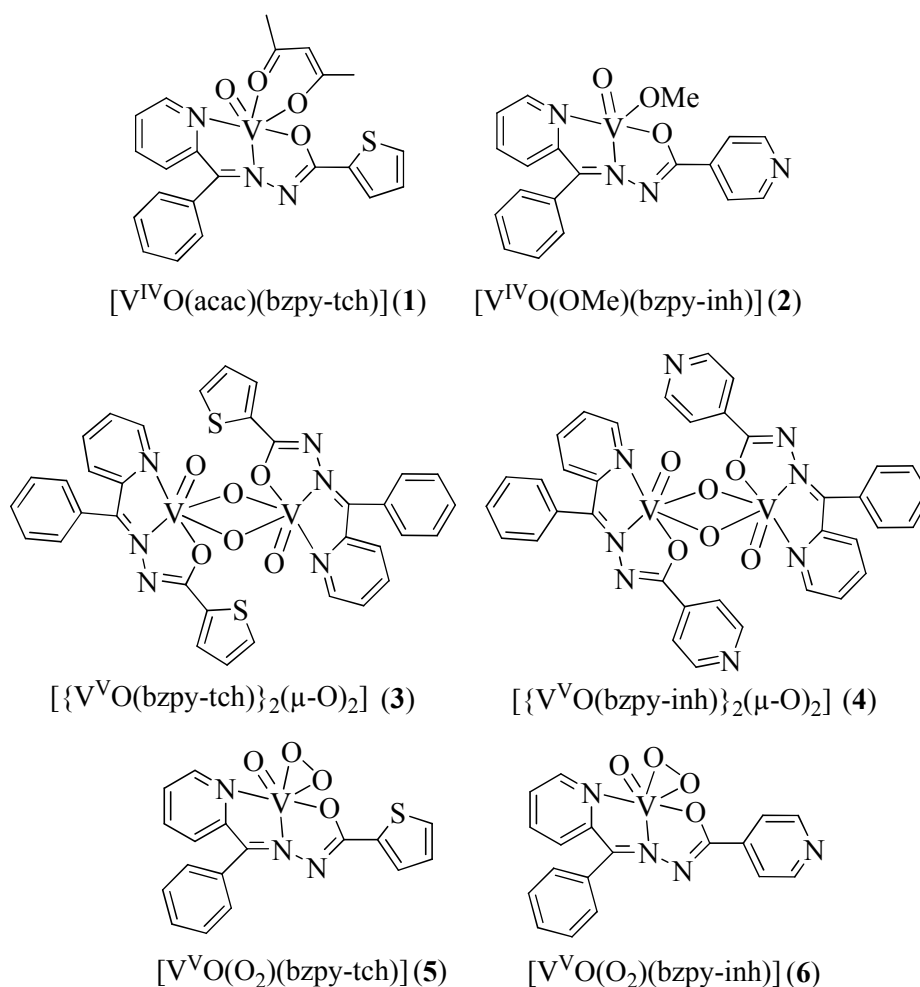
$${}^a R_1 = \frac{\sum ||F_o| - |F_c||}{\sum |F_o|} \cdot {}^b wR_2 = \left\{ \frac{\sum [w(|F_o|^2 - |F_c|^2)]^2}{\sum [w(F_o^4)]} \right\}^{1/2}$$

Catalytic oxidation of isoeugenol

The polymer anchored catalyst precursors were immersed in acetonitrile for 2 h prior to the reaction. In a double neck round bottom flask, isoeugenol (0.82 g, 5 mmol) and 30% H_2O_2 (1.13 g, 10 mmol, 1.0 mL) were mixed in 7 mL of acetonitrile and after addition of appropriate catalyst (20 mg) the reaction mixture was heated in an oil bath at 80 °C with very gentle mechanical stirring (to avoid crushing of polymer beads) for 4 h. To monitor the progress of the reaction, samples were taken out at every 30 min interval using a syringe and analyzed by a gas chromatograph equipped with a FID detector.

Results and discussion

Scheme 2 provides an overview of the complexes described in this work and the structural formulae of the complexes are based on their characterization by elemental analysis, spectroscopy (IR, UV/Vis, EPR, 1H , ^{13}C and ^{51}V NMR) and for **3**, **4**, **5** and **6a** by single-crystal X-ray diffraction analyses.

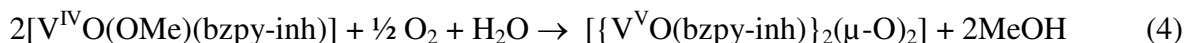
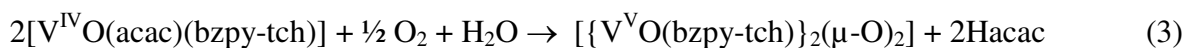


Scheme 2 Proposed structural formulae of the complexes reported in this work. The crystal of **6** corresponds to $[V^VO(O_2)(bzpy-inh)(H_2O)] \cdot 0.5MeOH$ **6a**. In solution it is probable that: (a) **3** and **4** predominantly exist as $[V^VO_2(bzpy-tch)(S)_n]$ and $[V^VO_2(bzpy-inh)(S)_n]$ (S = solvent molecule), with $n = 0$ or 1 ; (b) In the case of **5** and **6a** (see below) it is probable that they correspond to the structure shown in this scheme, with the possibility of containing a solvent molecule.

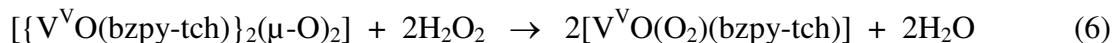
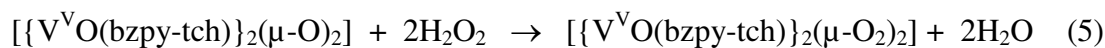
Synthesis, characterization and solid state characteristics

The precursor, $[V^{IV}O(acac)_2]$, reacts with an equimolar amount of similar compounds, Hbzpy-tch **I** and Hbzpy-inh **II** yielding two different types of complexes, $[V^{IV}O(acac)(bzpy-tch)]$ **1** (Eqn 1) and $[V^{IV}O(OMe)(bzpy-inh)]$ **2** (Eqn 2), respectively. However, upon their aerial oxidation in methanol and precipitation, they correspond to $[{V^VO(bzpy-tch)}_2(\mu-O)_2]$ **3** (Eqn 3) and $[{V^VO(bzpy-inh)}_2(\mu-O)_2]$ **4** (Eqn 4). Here, either solvent or steric hindrance had no definite

trend on the formulation of the complexes. As mentioned above we expect that in solution **3** and **4** are present as monomeric $V^V O_2$ -compounds.



Addition of H_2O_2 to methanolic solutions of **3** and **4** yielded the corresponding oxidomonoperoxidovanadium(V) complexes $[V^VO(bzpy-tch)]_2(\mu-O_2)_2$ **5** (Eqn 5) and $[V^VO(O_2)(bzpy-inh)]$ **6** (Eqn 6), respectively.

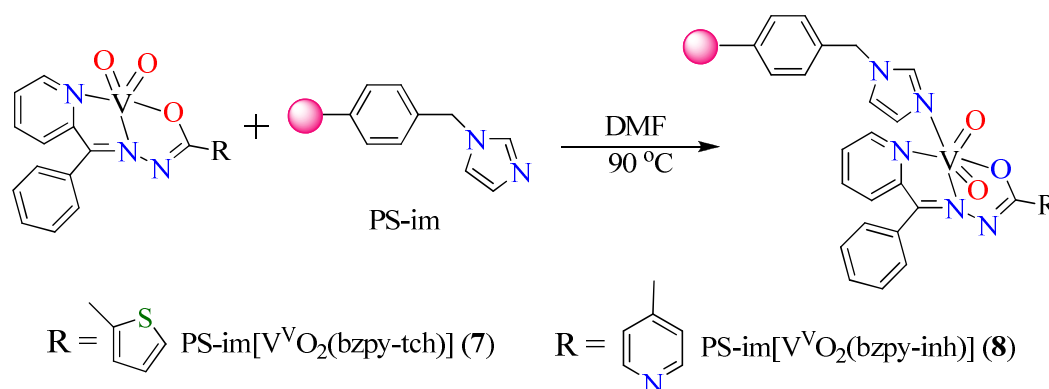


All complexes are fairly soluble in methanol, DMF and DMSO. Reaction of $[V^VO(bzpy-tch)]_2(\mu-O)_2$ **3** and $[V^VO(bzpy-inh)]_2(\mu-O)_2$ **4** with PS-im in DMF and ethyl acetate in the presence of triethylamine yielded the polymer-supported compounds: PS-im $[V^VO_2(bzpy-tch)]$ **7** and PS-im $[V^VO_2(bzpy-inh)]$ **8**, respectively. Here the available nitrogen atom of the imidazolomethylpolystyrene covalently binds to the vanadium atom of the complex (see Scheme 3). The metal ion loadings calculated from the obtained vanadium content (Table 2) for the polymer-supported complexes are also close to the value determined by thermogravimetric analyses (vide infra).

Table 2 Data of metal and loading in polymer-anchored complexes

Complexes	Metal ion loading ^a (mmol g ⁻¹ of resin) (obtained by ICP)	Metal ion loading ^a (mmol g ⁻¹ of resin) (obtained by TGA)
PS-im $[V^VO_2(bzpy-tch)]$ (7)	0.224	0.24
PS-im $[V^VO_2(bzpy-inh)]$ (8)	0.248	0.27

$$^a\text{Metal ion loading} = \frac{\text{Observed metal \%} \times 10}{\text{Atomic mass of metal}}$$



Scheme 3 synthetic scheme for the preparation of the polymer-supported complexes (only the monomeric forms of $\text{V}^{\text{V}}\text{O}_2$ -complexes are shown)

TGA studies

Thermal studies of $\text{V}^{\text{V}}\text{O}_2$ -complexes and their polymer-supported analogues, all dried at ca. 100 °C, were carried out to check their thermal stability. Both types of complexes are stable up to ca. 160 °C. The $\text{V}^{\text{V}}\text{O}_2$ -compounds start decomposing thereafter in multiple exothermic but overlapping steps, which are complete above ca. 520 °C to give V_2O_5 as the final product. The observed V_2O_5 contents of 23.8 % (for $[\{\text{V}^{\text{V}}\text{O}(\text{bzpy-tch})\}_2(\mu\text{-O})_2]$ **3**) and 23.3 % (for $[\{\text{V}^{\text{V}}\text{O}(\text{bzpy-inh})\}_2(\mu\text{-O})_2]$ **4**) match closely with the calculated values of 23.4 and 23.7%, respectively. The polymer-supported complexes $\text{PS-im}[\{\text{V}^{\text{V}}\text{O}_2(\text{bzpy-tch})\}]$ **7** and $\text{PS-im}[\text{V}^{\text{V}}\text{O}_2(\text{bzpy-inh})]$ **8** are thermally more stable, but show weight loss of 1 – 2% above ca. 120 °C, possibly due to residual moisture absorbed. The complete decomposition of complexes along with polymer occurs exothermically in two overlapping steps between ca. 200 – 500 °C. The final residue at 900 °C indicates the formation of V_2O_5 . The vanadium contents calculated are also included in Table 2, being in agreement with the values obtained by ICP-MS.

FE-SEM and EDAX analysis

FE-SEM images of PS-im and polymer anchored **7** and **8** show major morphological changes after anchoring; Fig. 1. Darkening of beads, significant increase in bead size and change in surface morphology of **7** and **8** as compared to PS-im were observed by FE-SEM studies. The presence of the peak for nitrogen in EDAX of PS-im confirms binding of imidazole to chloromethylated polystyrene. The peaks due to O and V other than N also confirm the presence of the vanadium complex on the surface of PS-im beads; Fig. 2. The average vanadium content obtained by EDAX by spotting two particular places yielded $0.20 \pm 0.02 \text{ mmol g}^{-1}$ of resin for **7** and $0.21 \pm 0.03 \text{ mmol g}^{-1}$ of resin for **8** which is close to the data of ICP-MS and TGA.

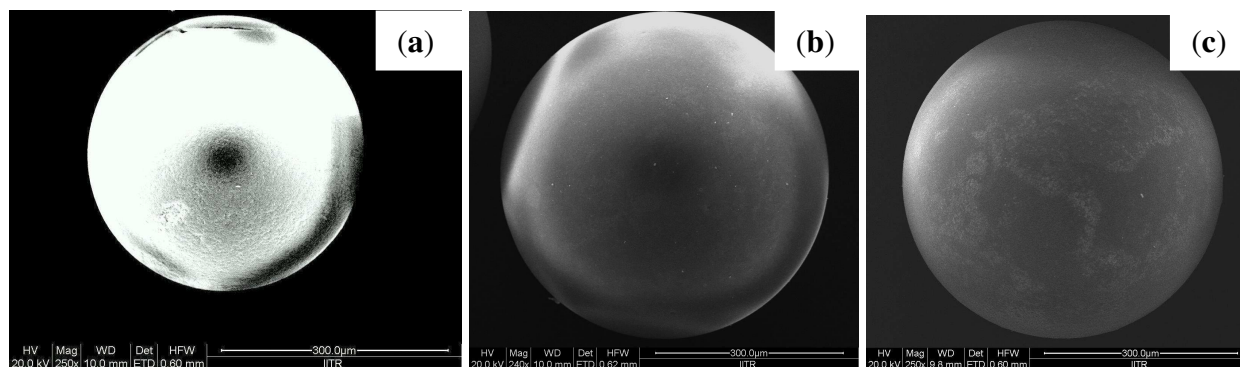


Fig. 1 Field emission scanning electron micrographs of PS-im (a), PS-[V^VO₂(bzpy-tch)] (b) and PS-[V^VO₂(bzpy-inh)] (c).

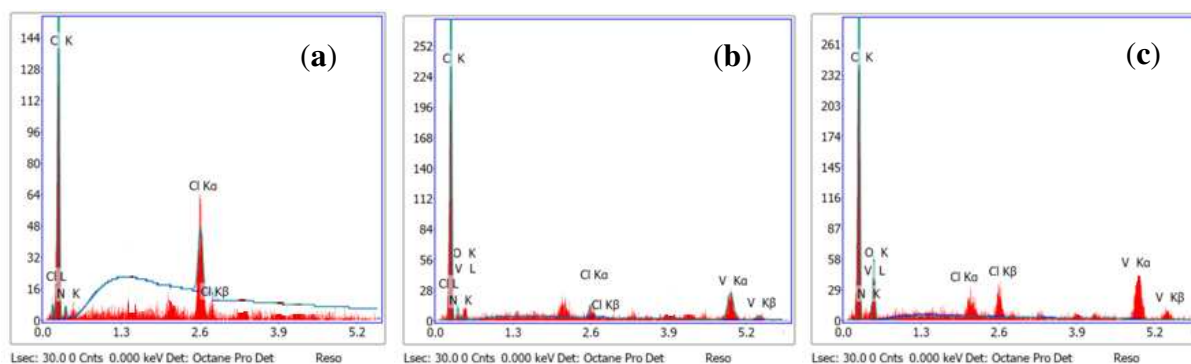


Fig. 2 Energy dispersive X-ray analysis graphs of PS-im (a), PS-[V^VO₂(bzpy-tch)] (b) and PS-[V^VO₂(bzpy-inh)] (c).

AFM study

AFM images (Fig. 3, left) of imidazolomethylpolystyrene beads show morphological changes before and after complex anchoring. The surface roughness and mean height as measured by AFM are 83.1 nm and 362.5 nm, respectively, for PS-im, whereas these values decrease after reaction of PS-im with V^V -complexes **3** and **4**, which confirm that the complexes are immobilized in the pores of PS-im beads,²¹ thereby reducing the surface roughness (surface roughness and mean height for PS-im[$V^V O_2$ (bzpy-tch)] **7** are: 25.6 nm, 149.7 nm, respectively, and for PS-im[$V^V O_2$ (bzpy-inh)] **8** are 19.7 nm, 100.3 nm, respectively) (Fig. 3, right side). Comparatively lower surface roughness and mean height in **8** than **7** indicates²¹ a more metal complex anchoring in the pores of **8**, this observation is also in agreement with the vanadium content obtained from ICP-MS, TGA and EDAX.

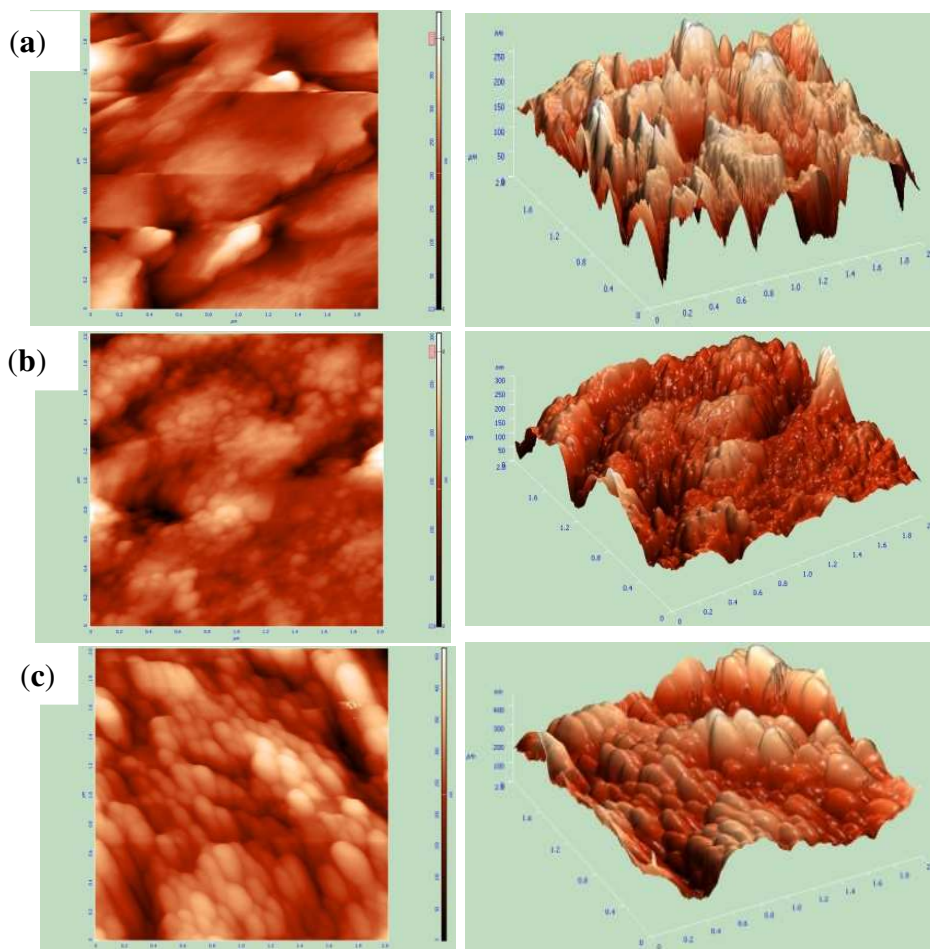


Fig. 3 AFM images (left) and respective 3D-views (right side) of PS-im (a), PS-[$V^V O_2$ (bzpy-tch)] (b) and PS-[$V^V O_2$ (bzpy-inh)] (c).

Molecular structure of complexes **3-5** and **6a**

The asymmetric unit of **3** contains two halves of two dinuclear complexes, while only one half of one dinuclear complex in the structure of **4**. The asymmetric unit of **6a** contains one peroxido complex and half methanol molecule. In all these compounds bzpy-tch and bzpy-inh ligands act as ONN donors. Table 3 includes selected bond lengths and angles.

Complex **3** crystallized from DMF and **4** from methanol as yellow prisms. Figs. 4 and 5 show their representation. The X-ray structure analysis of **4** shows two complexes with difference twist of the phenyl groups. The structures of **3** and **4** show that each V^V-center is six-coordinated in a distorted octahedral geometry, with terminal oxygen atoms, O3 (O3A by symmetry transformation) and O5, only in compound **3**, (O5A by symmetry transformation), and two bridging oxygen atoms, O2 (by symmetry transformation O2A) and O6, only in compound **3**, (O6A by symmetry transformation). O2 is strongly bound to V1 [V1–O2, 1.655(2) Å in **3** and 1.662(2) Å in **4**] and O6 to V2 [V2–O6, 1.662(2) Å in **3**] (Table 3), confirming that the V–μ-oxido bonds trans to the azomethine groups are also quite strong, having a somewhat weakened double bond character. O2A is weakly associated with V1 [V1–O2A, 2.358(2) Å in **3** and 2.340(2) Å in **4**] and O6A with V2 [V2–O6A, 2.327(2) Å in **3**] (Figures 4 and 5). The remaining three coordination sites are occupied by the pyridine N atoms [V1–N1, 2.104(3) Å in **3** and 2.113(3) Å in **4** and V2–N4, 2.110(3) Å in **3**], azomethine N atoms [V1–N2, 2.119(3) Å in **3** and 2.128(3) Å in **4**, and V2–N5, 2.122(3) Å in **3**] and ketonic O atoms [V1–O1, 1.956(2) Å in **3** and 1.972(2) Å in **4**, and V2–O4, 1.963(2) Å in **3**]. The V–V distances are V1–V1A, 3.158 Å and V2–V2A, 3.143 Å in **3**, and V1–V1A, 3.132 Å in **4**, and globally the O–V–O angles are similar to those observed in other compounds.²² Within the possible configurations for the [OV(μ-O)₂VO]⁺ core in complexes consisting of two edge-sharing octahedrally coordinated oxidovanadium centers, we can classify those found here as *anti*-coplanar.^{23,24} The vanadium atoms are displaced by about 0.0923 Å in **3** and about 0.2007 Å in **4** from the planes constituted for the atoms (C1, C2, C3, N1, N2, N3, C14, C15, C16, C17 in **3** and C1, C2, C3, N1, N2, N3, C15, C16, C17, C18 in **4**), which present a deviation from planarity of 0.0575(26) Å in **3** and 0.0518(24) Å in **4**.

Compound **5** crystallized from methanol as orange prisms and Figure 6A depicts an ORTEP representation. The complex is a dinuclear species containing two V^V-centers. The

vanadium centers adopt a distorted seven-coordinated pentagonal bipyramidal geometry with the bzpy-tch ligand bound through the pyridine-N atom [V1–N1, 2.120(4) Å], the azomethine-N atom [V1–N2, 2.089(4) Å] and one doubly bonded oxido ligand [V1–O1, 1.985(3) Å]. Each V^V is coordinated to one O₂²⁻ ligand and the two peroxido ligands also act as a monodentate bridge between the two V^V-centers. The V-V interatomic distance in the dinuclear assembly is 3.396 Å, and the distances to peroxide-O atoms acting as bridges are [V1–O2, 1.877(3) Å and V1-O2A, 2.419(3) Å]. Such peroxido bridges are very unusual in literature.²⁵

Compound **6a** crystallized from methanol as orange prisms and Fig. 6B depicts an ORTEP representation. In the molecular structure, the vanadium center adopts a distorted seven-coordinated pentagonal bipyramidal geometry with the bzpy-inh ligand coordinated through the pyridine N atom [V1–N1, 2.147(4) Å], azomethine N atom [V1–N2, 2.108(4) Å] and ketonic O atom [V1–O1, 2.021(3) Å]. One water molecule and two peroxido-O atoms, O4 and O5, are also coordinated to the V^V-center. The peroxido O-O distance of 1.439(4) Å lies within the range (1.38-1.45 Å) of the majority of compounds containing the peroxido ligand.^{3b} The V-O_{water} bond trans to the oxido-O atom is significantly longer [V1-O2, 2.256(3) Å]. The vanadium atom is displaced by about 0.1288 Å from the plane constituted by atoms: C1, C2, C3, N1, N2, N3, C15, C16, C17, C18, which presents a deviation from planarity of 0.0681(38) Å. Intermolecular hydrogen bonds exist between the coordinated water molecule and other complexes in the crystal packing (see Table 4). In the crystal packing of **6a**, the methanol molecule is implied in a symmetry operation (inversion centre at [0, 0, 0]), and can be present as a disordered molecule without refinement.

Table 3 Bond lengths [\AA] and angles [$^\circ$] for [$\{\text{V}^{\text{V}}\text{O}(\text{bzpy-tch})\}_2(\mu\text{-O})_2$] (**3**), [$\{\text{V}^{\text{V}}\text{O}(\text{bzpy-inh})\}_2(\mu\text{-O})_2$] (**4**), [$\{\text{V}^{\text{V}}\text{O}(\text{bzpy-tch})\}_2(\mu\text{-O}_2)_2$] (**5**) and for [$\text{V}^{\text{V}}\text{O}(\text{O}_2)(\text{bzpy-inh})(\text{H}_2\text{O})\cdot 0.5\text{MeOH}$] (**6a**)

Bond lengths	3 (1018367)	4 (1018368)	5 (1018365)	6a (1018366)
V(1)-O(1)	1.956(2)	1.972(2)	1.985(3)	2.021(3)
V(1)-O(2)	1.655(2)	1.662(2)	1.877(3)	2.256(3)
V(1)-O(2A)#1			2.419(3)	
V(1)-O(3)	1.613(2)	1.615(2)	1.588(3)	1.593(3)
V(1)-O(4)			1.862(3)	1.876(3)
V(1)-O(5)				1.855(3)
V(1)-N(1)	2.104(3)	2.113(3)	2.120(4)	2.147(4)
V(1)-N(2)	2.119(3)	2.128(3)	2.089(4)	2.108(4)
V(1)-O(2A)#2	2.358(2)	2.340(2)		
V(2)-O(5)	1.615(2)			
V(2)-O(6)	1.662(2)			
V(2)-O(4)	1.963(2)			
V(2)-N(4)	2.110(3)			
V(2)-N(5)	2.122(3)			
V(2)-O(6A)#3	2.327(2)			
O(4)-O(5)				1.439(4)
Angles	3	4	5	6a
O(3)-V(1)-O(2)	107.21(12)	107.01(11)	108.66(17)	169.43(15)
O(3)-V(1)-O(1)	98.48(11)	98.89(10)	100.91(15)	97.40(15)
O(2)-V(1)-O(1)	105.34(11)	105.19(10)	121.99(13)	85.42(12)
O(3)-V(1)-N(1)	95.78(11)	93.48(10)	88.45(16)	91.57(15)
O(2)-V(1)-N(1)	98.47(11)	100.21(10)	83.01(16)	80.64(13)
O(1)-V(1)-N(1)	147.06(10)	146.93(9)	147.37(16)	146.00(14)
O(3)-V(1)-N(2)	101.60(11)	98.89(11)	99.09(17)	92.76(16)
O(2)-V(1)-N(2)	150.73(11)	153.68(11)	143.05(16)	78.18(13)
O(1)-V(1)-N(2)	74.86(10)	74.70(9)	74.03(15)	73.89(13)
N(1)-V(1)-N(2)	73.26(10)	73.14(9)	73.65(17)	72.97(14)
O(3)-V(1)-O(5)				103.64(16)
O(3)-V(1)-O(4)			101.63(16)	104.05(16)
O(5)-V(1)-O(4)				45.36(13)
O(5)-V(1)-O(1)				126.54(14)
O(4)-V(1)-O(1)			81.37(13)	82.13(13)
O(5)-V(1)-N(2)				150.60(15)
O(4)-V(1)-N(2)			150.35(15)	152.30(15)
O(5)-V(1)-N(1)				82.23(14)
O(4)-V(1)-N(1)			127.62(17)	127.30(14)
O(5)-V(1)-O(2)				82.50(13)

O(4)-V(1)-O(2)			44.90(13)	86.40(13)
O(3)-V(1)-O(2A)#2	174.81(10)	#4 174.22(10)	#1 173.49(15)	
O(4)-V(1)-O(2A)			# 1 84.84(13)	
O(2)-V(1)-O(2A)#2	77.63(11)	#4 78.32(10)	#1 76.34(14)	
O(1)-V(1)-O(2A)#2	81.79(9)	#4 81.57(8)	#1 79.28(12)	
N(1)-V(1)-O(2A)#2	81.46(9)	#4 83.23(9)	#1 88.05(13)	
N(2)-V(1)-O(2A)#2	73.42(9)	#4 75.63(8)	#1 74.65(13)	
O(5)-V(2)-O(6)	106.55(12)			
O(5)-V(2)-O(4)	98.91(11)			
O(6)-V(2)-O(4)	105.87(10)			
O(5)-V(2)-N(4)	95.11(11)			
O(6)-V(2)-N(4)	99.38(11)			
O(4)-V(2)-N(4)	146.09(10)			
O(5)-V(2)-N(5)	100.73(12)			
O(6)-V(2)-N(5)	152.29(11)			
O(4)-V(2)-N(5)	74.06(10)			
N(4)-V(2)-N(5)	73.07(10)			
O(5)-V(2)-O(6A)#3	175.32(10)			
O(6)-V(2)-O(6A)#3	77.28(10)			
O(4)-V(2)-O(6A)#3	82.39(9)			
N(4)-V(2)-O(6A)#3	81.49(9)			
N(5)-V(2)-O(6A)#3	75.25(9)			
V(1)-O(2)-V(1A)#2	102.37(11)	#4 101.68(10)		
V(2)-O(6)-V(2A)#3	102.72(10)		#1 103.66(14)	

Symmetry transformations used to generate equivalent atoms:

#1 -x+1,-y,-z+1 #2 -x+1,-y+1,-z+2 #3 -x+1,-y+2,-z+1 #4 -x+1,-y,-z+1

Table 4 Hydrogen bonds for $[V^V O(O_2)(bzpy-inh)(H_2O)] \cdot 0.5MeOH$ (**6a**).

D-H...A	d(D-H)	d(H...A)	d(D...A)	<(DHA)
O(2)-H(2OA)...N(4)#5	1.03	1.78	2.784(5)	167.2
O(2)-H(2OB)...O(4)#6	1.00	1.87	2.863(5)	170.5
O(2)-H(2OB)...O(5)#6	1.00	2.44	3.343(5)	149.1

Symmetry transformations used to generate equivalent atoms:

#5 -x,-y+1,-z #6 -x+1,-y+1,-z+1

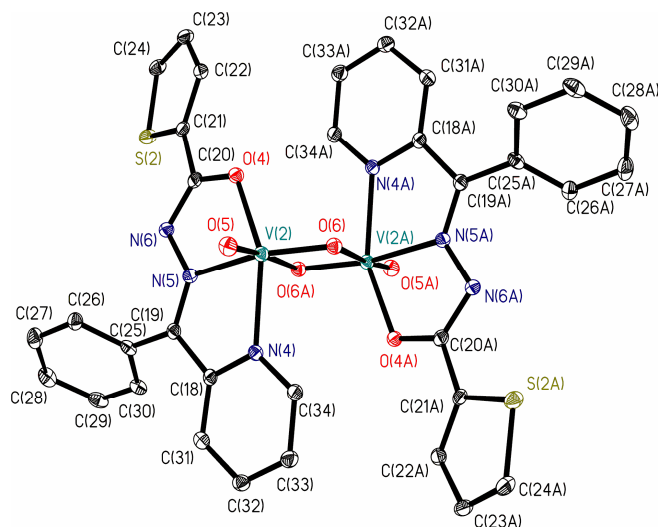


Fig. 4 ORTEP plot of $[\{V^VO(bzpy-tch)\}_2(\mu-O)_2]$ (**3**) (CCDC code 1018367). All the non-hydrogen atoms are presented by their 30% probability ellipsoids. Hydrogen atoms are omitted for clarity.

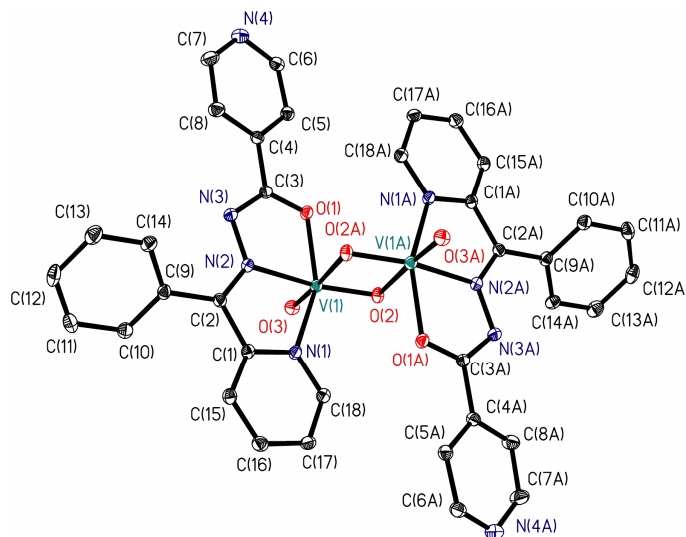


Fig. 5 ORTEP plot of $[\{V^VO(bzpy-inh)\}_2(\mu-O)_2]$ (**4**) (CCDC code 1018368). All the non-hydrogen atoms are presented by their 30% probability ellipsoids. Hydrogen atoms are omitted for clarity.

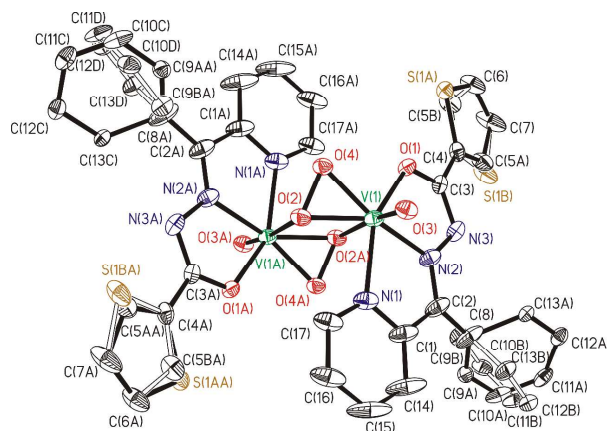


Fig. 6A ORTEP plot of $[\{V^V O(bzpy-tch)\}_2(\mu-O)_2]$ (**5**) (CCDC code 1018365). All non-hydrogen atoms are presented by their 30% probability ellipsoids. Hydrogen atoms are omitted for clarity.

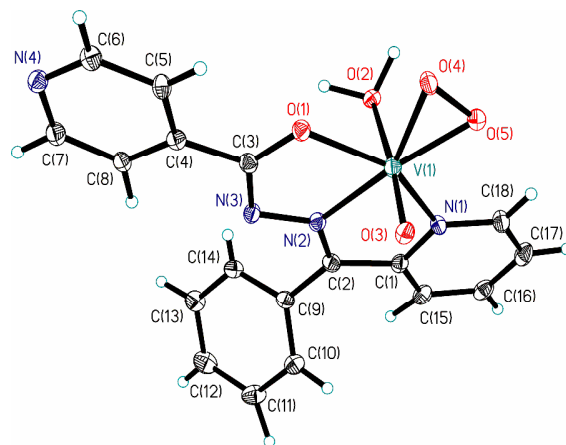


Fig. 6B ORTEP plot of $[V^V O(O_2)(bzpy-inh)(H_2O)] \cdot 0.5MeOH$ (**6a**) (CCDC code 1018366). All the non-hydrogen atoms are presented by their 30% probability ellipsoids; the MeOH unit is not shown.

IR spectral studies

Selected spectral IR data of the compounds are presented in Table 5. The $V^{IV}O$ -complexes exhibit one sharp band at $948\text{--}989\text{ cm}^{-1}$ due to $\nu(V=O)$ mode. The dinuclear $[(V^V O)_2(\mu-O)_2]^{2+}$ complexes **3** and **4** exhibit one sharp band at 936 cm^{-1} due to $\nu(V=O)$ and a broad band at $856\text{--}870\text{ cm}^{-1}$ assigned to $\nu[V-(\mu-O)-V]$.²⁶ The peroxido compounds **5** and **6**

exhibit a sharp band at 958–967 cm^{-1} due to $\nu(\text{V}=\text{O})$. In addition they exhibit three active vibrational bands at 920–923, 661–662 and 571–575 cm^{-1} due to the peroxido moiety, which may be assigned to the O–O intra stretching, asymmetric $\text{V}(\text{O}_2)$ stretching and symmetric $\text{V}(\text{O}_2)$ stretching, respectively.²⁷ All these signatures indicate the η^2 -coordination of the peroxido ligand.

Table 5 IR spectral data (cm^{-1}) of ligands and complexes. The assignments were made by comparison with previous studies, which include DFT calculated vibrational frequencies²⁶

Compounds	$\nu(\text{NH})$	$\nu(\text{C}=\text{O})$	$\nu(\text{C}=\text{N})$	$\nu(\text{V}=\text{O})/[\text{V}-(\mu\text{-O})\text{-V}]$
1 Hbzytch I	3053	1667	1637	-
2 Hbzyinh II	3062	1690	1635	-
3 $[\text{V}^{\text{IV}}\text{O}(\text{acac})(\text{bzytch})] \mathbf{1}$	-	-	1593	948
4 $[\text{V}^{\text{IV}}\text{O}(\text{OMe})(\text{bzyinh})] \mathbf{2}$	-	-	1589	989
5 $[\{\text{V}^{\text{V}}\text{O}(\text{bzytch})\}_2(\mu\text{-O})_2] \mathbf{3}$	-	-	1591	936, 856
6 $[\{\text{V}^{\text{V}}\text{O}(\text{bzyinh})\}_2(\mu\text{-O})_2] \mathbf{4}$	-	-	1590	936, 870
7 $[\{\text{V}^{\text{V}}\text{O}(\text{bzytch})\}_2(\mu\text{-O}_2)_2] \mathbf{5}^{\text{a}}$	-	-	1586	967
8 $[\text{V}^{\text{V}}\text{O}(\text{O}_2)(\text{bzyinh})] \mathbf{6}^{\text{a}}$	-	-	1585	958
9 PS-im $[\text{V}^{\text{V}}\text{O}_2(\text{bzytch})] \mathbf{7}$	-	-	1609	917
10 PS-im $[\text{V}^{\text{V}}\text{O}_2(\text{bzyinh})] \mathbf{8}$	-	-	1609	940

^a Bands due to peroxide moiety: Complex **5**: 923, 662 and 571 cm^{-1} ; Complex **6**: 920, 661 and 575 cm^{-1} .

The IR spectra of the ligands exhibit three sharp bands at 3053–3062, 1667–1690 and 1635–1637 cm^{-1} due to $\nu(\text{NH})$, $\nu(\text{C}=\text{O})$ (of the hydrazide moiety) and $\nu(\text{C}=\text{N})$ (azomethine), respectively. The first two bands are indicative of their ketonic nature in the solid state. Non-presence of these bands in the IR spectra of all complexes indicates their enolisation and replacement of H by the metal ion. The $\nu(\text{C}=\text{N})$ show up at lower wave numbers in all complexes, indicating the coordination of the azomethine nitrogen to the vanadium. The coordination of pyridinic nitrogen of benzoylpyridine residue to vanadium could not be assigned unequivocally due complexity of the spectra in the relevant region. However, taking into account

the single crystal X-ray diffraction study (vide supra) it is clear that the ring nitrogen atom takes part in coordination. All polymer anchored complexes exhibit spectral patterns similar to monomeric $[V^V O_2]^+$ complexes but with weak intensity.

Electronic spectral studies

Electronic absorption spectra (UV-Vis) for all ligands and neat complexes were recorded in methanol; the spectra in the visible region for the $V^{IV}O$ -complexes were recorded in DMF. Figs. 7 and 8 depict spectra of peroxido and polymer-supported complexes. The absorption maxima with their extinction coefficients (wherever possible) are given in Table 6. The ligand Hbzpy-inh (**II**) display three bands at 203, 265 and 317 nm, while Hbzpy-tch (**I**) exhibits one additional band at 247 nm, along with the above bands at nearly the same positions. These bands are assignable to $\varphi \rightarrow \varphi^*$, $\pi \rightarrow \pi^*$ and $n \rightarrow \pi^*$, transitions; the band at 247 nm probably also corresponds to a $\pi \rightarrow \pi^*$ transition. These bands are also observable in the spectra of the V^V -complexes with some variations in their positions. All complexes also display a medium intensity band in the visible region at *ca.* 400 nm which is assigned to a ligand-to-metal charge-transfer (LMCT) transition. In addition, the $V^{IV}O$ -complexes display two bands at 525 and 760 nm in **1**, and at 645 and 805 nm in **2**, which are assigned to d-d transitions. Oxidoperoxidovanadium(V) complexes exhibit LMCT bands at same position as observed in the corresponding $V^V O_2$ -complexes, but these bands at *ca.* 400-420 nm have higher intensity. The UV-Vis spectra of the polymer-supported complexes do not depict clearly distinct bands (see Figure 8), but bands are noticeable which, in general, appear at nearly the same positions as those observed for the corresponding V^V -complexes. All these suggest the immobilization of these V^V -complexes on the polymer matrix.

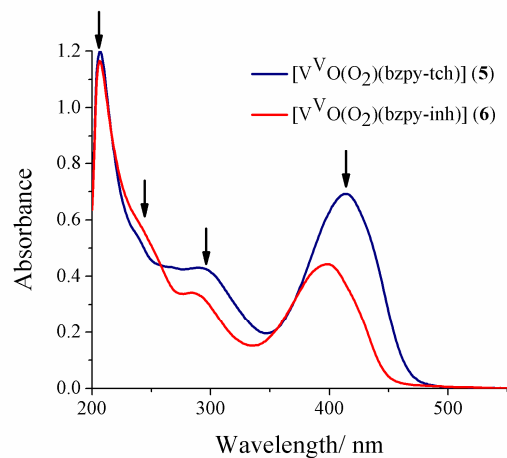


Fig. 7 Electronic spectra of oxidoperoxidovanadium(V) complexes **5** and **6** recorded in methanolic solution. Solution concentrations of complexes: **5**: 3.3×10^{-5} M and **6**: 3.1×10^{-5} M respectively.

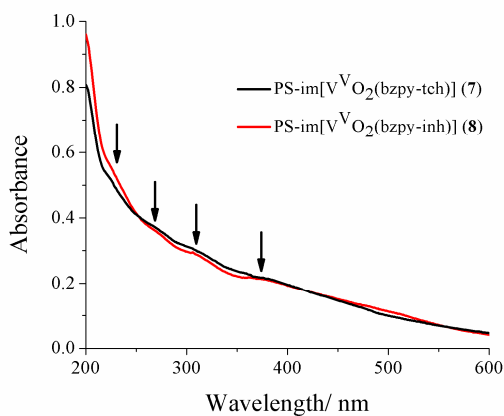


Fig. 8 Electronic spectra of polymer-supported V^V -complexes **7** and **8** after being dispersed in Nujol.

Table 6 Electronic spectral data of the compounds prepared

Compounds	Solvent	λ_{\max}/nm ($\epsilon/\text{M}^{-1} \text{cm}^{-1}$)
Hbzpy-tch I	MeOH	203 (2.73×10^4), 247 (1.83×10^4), 271 (1.85×10^4), 320 (2.15×10^4)
Hbzpy-inh II	MeOH	203 (2.57×10^4), 265 (1.45×10^4), 317 (5.9×10^3)
[V ^{IV} O(acac)(bzpy-tch)] 1	MeOH	206 (1.40×10^4), 271 (1.44×10^4), 306 (1.37×10^4), 402 (1.6×10^3)
	DMF	525 (74), 766 (16)
[V ^{IV} O(OMe)(bzpy-inh)] 2	MeOH	208 (2.93×10^4), 222 (3.06×10^4), 272 (1.79×10^4), 340 (1.52×10^4), 420 (5.0×10^3)
	DMF	645 (91), 805 (15)
[{V ^V O(bzpy-tch)} ₂ (μ -O) ₂] 3	MeOH	205 (2.50×10^4), 240 (1.60×10^4), 279 (1.34×10^4), 306 (1.50×10^4), 418 (1.05×10^4)
[{V ^V O(bzpy-inh)} ₂ (μ -O) ₂] 4	MeOH	206 (1.22×10^4), 238 (sh) (7.5×10^3), 256 (6.7×10^3), 306 (1.15×10^4), 405 (6.1×10^3),
[{V ^V O(bzpy-tch)} ₂ (μ -O ₂) ₂] 5	MeOH	206 (3.45×10^4), 240 (1.41×10^4), 290 (1.15×10^4), 415 (1.70×10^4)
[V ^V O(O ₂)(bzpy-inh)] 6	MeOH	206 (3.83×10^4), 249 (1.55×10^4), 283 (1.04×10^4), 400 (1.24×10^4)
PS-im[V ^V O ₂ (bzpy-tch)] 7	Nujol	235, 270, 308, 395
PS-im[V ^V O ₂ (bzpy-inh)] 8	Nujol	231, 265, 309, 380

¹H NMR spectral studies

The mode of the coordination was also confirmed by measuring the ¹H NMR of the ligands and complexes. The ¹H NMR spectra (Supporting information, Figs. S1 – S4) were recorded in DMSO-d₆ and the data are presented in Table 7. A broad signal appearing at δ values 8.94 and 10.16 ppm in Hbzpy-tch (**I**) and Hbzpy-inh (**II**), respectively, due to the –NH– proton is not detected in the spectra of the complexes, which demonstrates the enolization and consequent replacement of H and coordination of the enolate oxygen. Signals for aromatic protons of the ligands and complexes appear within the expected region but substantial downfield shift was

observed for some signals in the complexes. For **3** and **4**, a downfield shift of $\Delta\delta = 0.83$ ppm (in **3**) and 0.24 ppm (in **4**) $\{\Delta\delta = [\delta(\text{complex}) - \delta(\text{ligand})]\}$ in the signal of the protons adjacent to pyridyl nitrogen (of bzpy) in comparison to the free ligand, confirms its coordination. For **5** and **6** the signal for the same proton appears more downfield shifted ($\Delta\delta = 0.86$ ppm in **5** and 1.03 ppm in **6**), which can be attributed to the presence of peroxido ligand.

Table 7 ^1H NMR spectral data of ligand and complexes

Compounds ^a	-NH	Aromatic H		
		(pyridyl ring) _{bzpy}	(phenyl ring) _{bzpy}	(pyridyl ring) _{inh} / (thiophene ring) _{tch}
Hbzpy-tch I	8.94 (s, 1H)	8.06-8.02 (m, 1H), 7.58-7.56 (m, 2H), 7.40-7.36 (m, 1H)	7.65-7.62 (m, 2H), 7.52-7.51 (m, 3H)	7.99-7.95 (m, 2H), 7.26- 7.25 (m, 1H)
Hbzpy-inh II	10.16 (s, 1H)	8.68-8.67 (m, 1H), 8.056- 8.024 (m, 1H), 7.98-7.97 (d, 1H), 7.96-7.94 (m, 1H)	7.65-7.63 (m, 2H), 7.53-7.50 (m, 3H)	8.71-8.69 (d, 2H), 7.74- 7.73 (d, 2H)
[{V ^V O(bzpy-tch)} ₂ (μ -O) ₂] 3	—	8.89-8.88 (d, 1H), 8.28-8.24 (m, 1H), 7.82-7.80 (m, 2H)	7.78-7.76 (m, 1H), 7.68-7.65 (m, 4H)	7.87-7.86 (d, 1H), 7.71- 7.70 (d, 1H), 7.20-7.18 (m, 1H)
[{V ^V O(bzpy-inh)} ₂ (μ -O) ₂] 4	—	8.92-8.91 (d, 1H), 8.31-8.28 (m, 1H), 7.87-7.86 (d, 1H), 7.86-7.85 (m, 1H)	7.83-7.80 (m, 1H), 7.73-7.70 (m, 4H)	8.72-8.71 (d, 2H), 7.78- 7.76 (d, 2H)
[{V ^V O(bzpy-tch)} ₂ (μ -O) ₂] 5	—	9.69-9.68 (d, 1H), 8.30-8.27 (m, 1H), 7.81-7.77 (m, 2H)	7.66-7.62 (m, 5H)	7.96-7.93 (m, 1H), 7.61- 7.59 (d, 1H), 7.21-7.19 (m, 1H)
[V ^V O(O ₂)(bzpy-inh)] 6	—	9.71-9.72 (d, 1H), 8.33-8.28 (m, 1H), 8.01-7.99 (m, 1H), 7.70-7.68 (m, 1H)	7.67- 7.65 (m, 5H)	8.74-8.73 (d, 2H), 7.90- 7.89 (d, 2H)

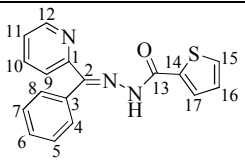
^a Letters given in parentheses indicate the signal structure: s = singlet, d = doublet and m = multiplet.

^{13}C NMR spectral studies

The binding modes of the ligands were further supported by the study of the coordination-induced ^{13}C NMR chemical shifts (SI Figs. S5 – S8). ^{13}C NMR signals were recorded in DMSO-*d*₆; their assignments are given in Tables 8 and 9. Significant downfield shifts, $\Delta\delta = [\delta(\text{complex}) - \delta(\text{ligand})]$ were observed in the signals of the carbon atoms in the vicinity of the coordinating atoms. Coordination of the enolate oxygen was indicated by a large downfield shift, $\Delta\delta = 20.44$ ppm in the signal of enolate carbon i.e. C13 in case of **3**, and $\Delta\delta = 23.62$ ppm in case of **4**.^{1b}

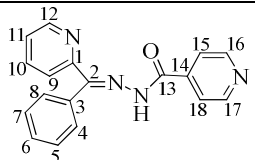
Similarly, the peak due to azomethine carbon, i.e. C2, also appeared at lower field in the spectra of **3** and **4** as compared to **I** and **II**. Even the signals due to carbon atoms C1 and C12 also showed noticeable downfield shifts in complexes **3** and **4**, confirming the coordination of the pyridyl-N atom of bzpy. Similar trends for carbon atoms C1, C2, C12 and C13 were observed in the spectra of complexes **5** and **6**. In ligands the peaks due to the carbon atoms of phenyl ring and thiophene or pyridyl ring appeared at the expected δ values, which also appeared in the ^{13}C NMR spectra of complexes **3**, **4**, **5** and **6**, but slightly shifted.

Table 8 ^{13}C NMR spectral data of Hbzpy-tch (**I**) and its complexes

	C1	C2	C12	C13	C4/C8	C5/C7	C3, C6, C9, C10, C11, C14, C15, C16, C17
Hbzpy-tch I	148.93	151.60	138.27	154.92	128.46	128.84	129.38, 124.96, 121.89, 131.45, 124.07, 136.81, 126.16, 128.88, 129.42
$[\{\text{V}^{\text{V}}\text{O}(\text{bzpy-tch})\}_2(\mu\text{-O})_2]$ 3 ($\Delta\delta$)	154.73 (5.80)	158.16 (6.56)	153.67 (15.40)	175.36 (20.44)	128.46	130.19	133.41, 128.43, 126.72, 134.00, 126.92, 143.10, 128.50, 131.11, 132.49
$[\{\text{V}^{\text{V}}\text{O}(\text{bzpy-tch})\}_2(\mu\text{-O}_2)_2]$ 5 ($\Delta\delta$)	151.79 (2.86)	155.75 (4.15)	149.93 (11.66)	173.91 (18.99)	128.51	129.81	132.21, 128.21, 125.77, 135.76, 126.32, 141.97, 129.69, 130.30, 131.62

$$^a\Delta\delta = [\delta(\text{complex}) - \delta(\text{ligand})]$$

Table 9 ^{13}C NMR spectral data of Hbzpy-inh (**II**) and its complexes

	C1	C2	C12	C13	C4/C8	C5/C7	C15/C18	C16/C17	C3, C6, C9, C10, C11, C14
Hbzpy-inh II	148.94	149.99	140.39	151.78	128.31	129.52	121.18	150.83	136.88, 128.31, 125.22, 137.26, 126.53, 138.51
$[\{\text{V}^{\text{V}}\text{O}(\text{bzpy-inh})\}_2(\mu\text{-O})_2]$ 4 ($\Delta\delta$)	153.79 (4.85)	154.41 (4.42)	143.16 (2.77)	175.40 (23.62)	128.53	130.25	122.04	150.41	131.29, 128.25, 127.28, 131.97, 127.56, 138.26
$[\text{V}^{\text{V}}\text{O}(\text{O}_2)(\text{bzpy-inh})]$ 6 ($\Delta\delta$)	154.78 (5.84)	155.43 (5.44)	150.14 (9.75)	175.87 (24.09)	128.60	129.82	122.36	150.41	130.61, 128.29, 126.52, 139.72, 127.02, 142.16

Electrospray ionization mass spectrometry

Compounds **1** to **4** were studied by ESI-MS (positive mode) also as a means to observe what species are formed in acetonitrile solution, the solvent used in the catalytic experiments. The respective spectra are included in the Supporting Material (Figs. S9 -S11). For compound **1**, one of the major species detected is assigned to the sodium adduct of HBzpy-tch ($[\text{Na}(\text{HBzpy-tch})]^+$, $m/z = 330$). The species at $m/z=767$ may be assigned to either the dinuclear molecular ion $[\{\text{V}^{\text{IV}}\text{O}(\text{bzpy-tch})\}_2\text{O}]^+$ or the mixed valence species $[\{\text{V}^{\text{V}}\text{O}(\text{bzpy-tch})\}\text{O}\{\text{V}^{\text{IV}}\text{O}(\text{bzpy-tch})\}]^+$. The species at $m/z=844$ may be due to the adduct of two acetonitrile molecules with either one of the species assigned to $m/z=762$.

For **2**, two of the major species detected correspond to $\text{H}_2\text{Bzpy-inh}^+$ ($m/z=303$) and the respective sodium adduct ($[\text{Na}(\text{HBzpy-inh})]^+$, $m/z = 325$). Minor species are assigned to the following: $[\text{Na}(\text{Bzpy-inh})]^+$ at $m/z= 365$; $[\text{H}\{\text{V}^{\text{V}}\text{O}_2(\text{bzpy-inh})(\text{inh})(\text{MeOH})_2\}]^+$ at $m/z=585$ and the respective acetonitrile adducts at $m/z= 627$ and 667 ; the species at $m/z=752$ may be assigned to the mixed valence species $[\{\text{V}^{\text{V}}\text{O}(\text{bzpy-inh})\}\text{O}\{\text{V}^{\text{IV}}\text{O}(\text{bzpy-inh})\}]^+$. For compound **3** the major species detected is assigned to $[\{\text{V}^{\text{V}}\text{O}(\text{bzpy-tch})\}\text{O}\{\text{V}^{\text{IV}}\text{O}(\text{bzpy-tch})\}]^+$ at $m/z=762$.

For compound **4**, the following species were assigned: the one at $m/z=309$ to the doubly charged $[\text{H}\{\text{V}^{\text{V}}\text{O}(\text{bzpy-inh})(\text{bzpy})(\text{H}_2\text{O})(\text{MeOH})\}]^{2+}$; the sodium adduct ($[\text{Na}(\text{HBzpy-inh})]^+$ is detected at $m/z = 325$; the species at $m/z=385$ is assigned to $[\text{H}\{\text{V}^{\text{V}}\text{O}_2(\text{bzpy-tch})\}]^+$; the species at $m/z=611$ is assigned to $[\text{V}^{\text{V}}\text{O}_2(\text{bzpy-tch})(\text{inh})(\text{CH}_3\text{CN})(\text{MeOH})(\text{H}_2\text{O})]^+$, the species at $m/z=752$ is assigned to the mixed valence species $[\{\text{V}^{\text{V}}\text{O}(\text{bzpy-inh})\}\text{O}\{\text{V}^{\text{IV}}\text{O}(\text{bzpy-inh})\}]^+$ and the species at $m/z=775$ is assigned to the mixed valence species $[\text{Na}\{\text{V}^{\text{IV}}\text{O}(\text{bzpy-inh})\}\text{O}\{\text{V}^{\text{IV}}\text{O}(\text{bzpy-inh})\}]^+$.

Overall, all compounds exhibit a tendency to aggregate into μ -oxido-bridged species even under the ESI-MS conditions. With the exception of compound **3**, the free ligand was detected in all cases. Ligand fragmentation was also observed with the isonicotinoylhydrazide compounds **2** and **4**, also suggesting their relatively lower stability when compared to **1** and **3**.

Electron paramagnetic resonance studies

Compounds $[\text{V}^{\text{IV}}\text{O}(\text{acac})(\text{bzpy-tch})]$ **1**, $[\text{V}^{\text{IV}}\text{O}(\text{MeO})(\text{bzpy-inh})]$ **2** were characterized by EPR, and the corresponding X-band spectra are depicted in Fig. 9. The V^{V} -compounds **3** and **4**, as well $\text{PS-}[\text{V}^{\text{V}}\text{O}_2(\text{bzpy-tch})]$ **7** and $\text{PS-}[\text{V}^{\text{V}}\text{O}_2(\text{bzpy-inh})]$ **8** were also analyzed by EPR in order to ascertain if the respective synthetic procedures afforded the complete oxidation of the precursor V^{IV} species. Interestingly, some initial samples of **4**, **7** or **8**, yielded EPR signals (Fig. S12). After further oxidation of the samples, no EPR signal was detected either for the solid samples of **4**, **7** or **8**, or for **3** and **4** in solution.

Table 10 depicts the spin Hamiltonian parameters obtained for compounds **1** and **2**, and Table S1 the spin Hamiltonian parameters corresponding to the V^{IV} -impurities present in the initial samples of **4**, **7** and **8**.

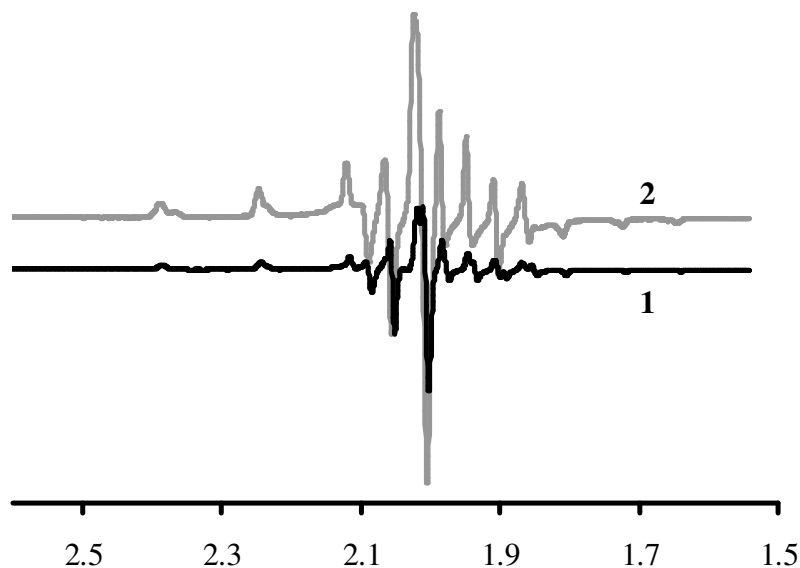


Fig. 9 First derivative of the EPR spectra measured for compounds **1** and **2** in DMF solution at 77 K.

Table 10 Spin hamiltonian parameters obtained by simulation²⁸ of the spectra of compounds **1** and **2** in frozen solutions of DMF at 77 K.

Compound	g_x, g_y	$A_x, A_y \times 10^4 \text{ cm}^{-1}$	g_z	$A_z \times 10^4 \text{ cm}^{-1}$	Donor atom set ²⁹⁻³¹
1	1.974, 1.979	61.7, 54.9	1.946	167.3	$N_{\text{imine}}, N_{\text{pyr}}, O_{\text{acac}}, O_{\text{ArO}}$
	1.981 ^a	57.4 ^a	1.950 ^a	167.5 ^a	or $N_{\text{imine}}, N_{\text{pyr}}, O_{\text{DMF}}, O_{\text{ArO}}$
2	1.982	57.6	1.951	167	$N_{\text{imine}}, N_{\text{pyr}}, O_{\text{DMF}}, O_{\text{ArO}}$
			1.951	159.4	$N_{\text{imine}}, N_{\text{pyr}}, O_{\text{RO}}, O_{\text{ArO}}$

^a Spectrum measured from a CH_2Cl_2 solution at 77 K.

The probable equatorial donor atom coordinated to the $\text{V}^{\text{IV}}\text{O}$ center were assigned using the additivity rule developed by Wüthrich and Chasteen.²⁹ For compounds **1** and **2** in DMF, the obtained spin Hamiltonian parameters, namely the A_z values, are in agreement with the expected tridentate donor atom sets, either $[N_{\text{imine}}, N_{\text{pyr}}, O_{\text{DMF}}, O_{\text{ArO}}]$, which includes also a coordinated solvent molecule, or $[N_{\text{imine}}, N_{\text{pyr}}, O_{\text{acac}}, O_{\text{ArO}}]$, as the contributions of O_{DMF} ($A_z(\text{DMF}) = 43.7 \times 10^4 \text{ cm}^{-1}$)³⁰ and ($A_z(\text{acac}) = 41.6 \times 10^4 \text{ cm}^{-1}$)³¹ do not really allow distinguishing between both binding sets. In fact, measuring the EPR spectrum in a CH_2Cl_2 solution, the A_z values do not change much, suggesting that in DMF solutions one of the O-acac^- atoms probably remains coordinated equatorially.

The spectrum of **2** shows also a minor species that exhibits z -component parameters ($g_z = 1.951$, $A_z = 159.4 \times 10^4$) consistent with a coordinated methoxido⁻ ligand. Thus the assigned donor atom set $[N_{\text{imine}}, N_{\text{pyr}}, O_{\text{RO}}, O_{\text{ArO}}]$ is in agreement with the expected formula of $[\text{V}^{\text{IV}}\text{O}(\text{MeO})(\text{bzpy-inh})]$. This compound was not soluble in CH_2Cl_2 to allow measuring its EPR spectrum in this non-coordinating solvent.

Reactivity of $[\text{V}^{\text{IV}}\text{O}(\text{acac})(\text{bzpy-tch})]$ **1** and $[\{\text{V}^{\text{V}}\text{O}(\text{bzpy-tch})\}_2(\mu\text{-O})_2]$ **3** towards H_2O_2

As described above, the oxidoperoxidovanadium(V) complexes **5** and **6** were isolated and characterized. The in-situ generation of the peroxido species in solution from the corresponding $\text{V}^{\text{IV}}\text{O}$ -complexes, by their treatment with H_2O_2 , was also followed by electronic absorption

spectroscopy, depicting very interesting spectral changes. Thus, at least two types of electronic spectral patterns were observed during the stepwise additions of one drop of a H_2O_2 solution (0.051 g of 30 % H_2O_2 taken in 15 mL of MeOH) to 25 mL of ca. 2.3×10^{-5} M solution of $[\text{V}^{\text{IV}}\text{O}(\text{acac})(\text{bzpy-tch})]$ (**1**) in MeOH. As shown in Fig. 10 for set (a), the band at 307 nm shifts to 321 nm with decrease in intensity, while the band at 271 nm increases its intensity without changing its λ_{max} . A weak band appearing at ca. 418 nm maintains its λ_{max} with slight decrease in intensity, while the band at ~ 204 nm maintains its position with a slight increase in intensity. Further additions of H_2O_2 causes no significant change in the λ_{max} of all bands, but there is a sharp increase in the intensity of the 204 nm band, together with only marginal increase in the intensities of the 271, 321 and 418 nm bands. We interpret these spectral changes as corresponding to: (a) oxidation of the $\text{V}^{\text{IV}}\text{O}$ -complex, yielding a V^{V} -species (**3** or most probably its mononuclear $\text{V}^{\text{V}}\text{O}_2$ -counterpart), followed by the generation of oxidoperoxidovanadium(V) species in solution.

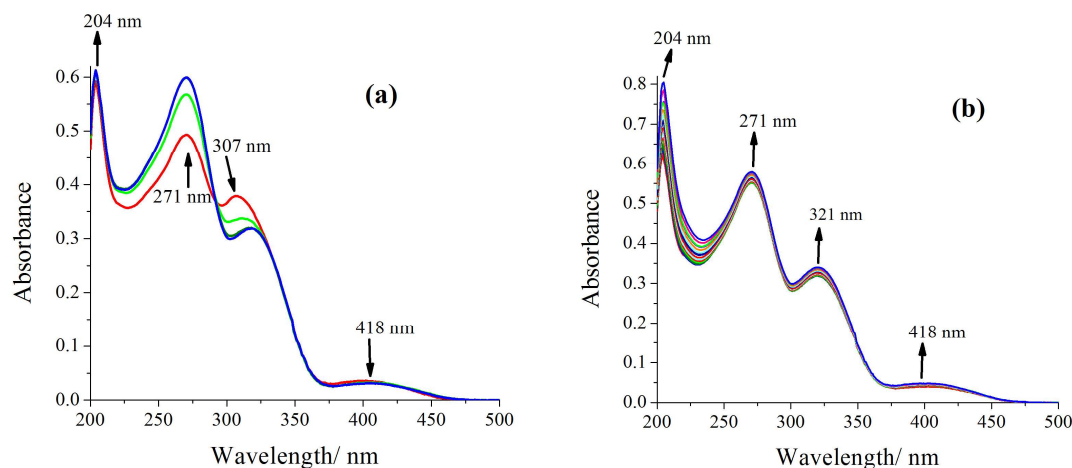


Fig. 10 Two sequential sets (a) and (b) of spectral changes obtained by stepwise one drop additions of a H_2O_2 solution (prepared from 0.051 g (0.45 mmol) of 30 % H_2O_2 dissolved in 15 mL of MeOH) to 25 mL of ca. 2.3×10^{-5} M solution of $[\text{V}^{\text{IV}}\text{O}(\text{acac})(\text{bzpy-tch})]$ **1** in MeOH.

The two d-d bands present at 570 and 766 nm are also sensitive towards H_2O_2 as observed by making similar titrations but with more concentrated solutions, in DMF. Stepwise

additions of a H₂O₂ solution (prepared from 0.051 g (0.45 mmol) of 30 % H₂O₂ dissolved in 15 mL of DMF) to 4 mL of a ca. 3.8×10^{-3} M solution of [V^{IV}O(acac)(bzpy-tch)] in DMF caused a considerable reduction in intensity of the band at 766 nm, followed by its flattening, while the band at 570 nm is substituted by a shoulder at ca. 540 nm, along with considerable increase in intensity (Fig. 11 (a)). Further additions of H₂O₂ caused considerable reduction in the intensity along with progressive disappearance of both bands (Fig. 11(b)).

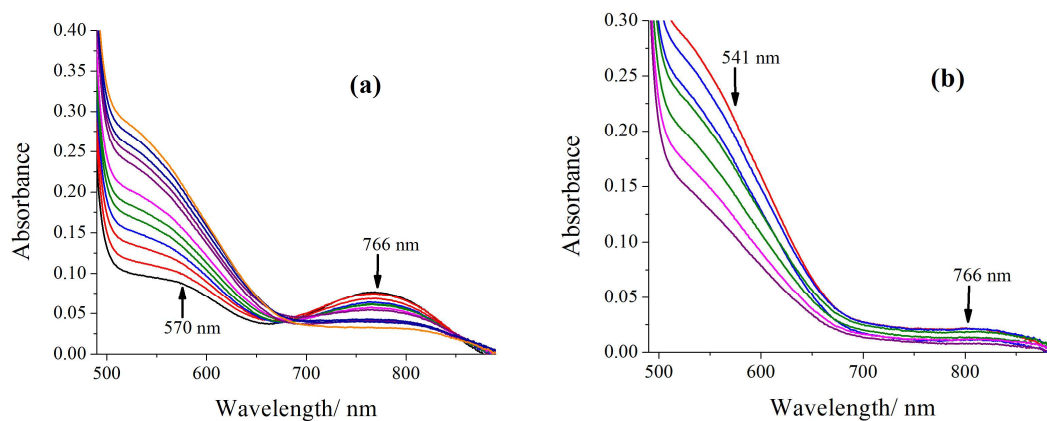


Fig. 11 Two sequential sets of spectral changes by stepwise one drop additions of a H₂O₂ solution (prepared from 0.051 g (0.45 mmol) of 30 % H₂O₂ in 15 mL of DMF) to 4 mL of ca. 3.8×10^{-3} M solution of [V^{IV}O(acac)(bzpy-tch)] in DMF. (a) showing flattening of 766 nm band and formation of a band at ca. 540 nm, and (b) emphasizing the flattening of both bands with progressive decrease in intensity.

Solutions of [$\{V^V O(bzpy-tch)\}_2(\mu-O)_2$] **3** in MeOH are also sensitive towards H₂O₂, as monitored by UV-Vis absorption spectroscopy. Again two different sequential sets of electronic spectral patterns were observed upon stepwise additions of a solution of H₂O₂ (prepared from 0.051 g (0.45 mmol) of 30 % H₂O₂ dissolved in 10 mL of MeOH) to 25 mL of ca. 6.0×10^{-5} M solution of [$\{V^V O(bzpy-tch)\}_2(\mu-O)_2$] in MeOH. In Fig. 12 (a) it is observed that the band at 418 nm continuously increases its intensity while the band at 306 nm decreases its intensity, but their

positions remain nearly same and an isosbestic point is observed at 332 nm. A shoulder at 238 nm shifts to 234 nm with slight decrease in intensity, while the band at 207 nm gains intensity.

Upon further additions of H₂O₂ (second set) the two bands at 418 and 306 nm gain intensity while maintaining their positions (Fig. 12(b)). The weak shoulder at 234 nm becomes less and less distinguishable by this increase in intensity, while the band at 207 nm only gains intensity. The initial spectrum of the 2nd set is similar to the UV-Vis spectrum recorded for [{V^VO(bzpy-tch)}₂(μ-O₂)₂] **5**. This observation suggests that the V^V-complex **3** initially changes to the corresponding V^VO(O₂)(L) species and then possibly converts into non-ligand containing V^VO(O₂)-(H₂O)_n species.

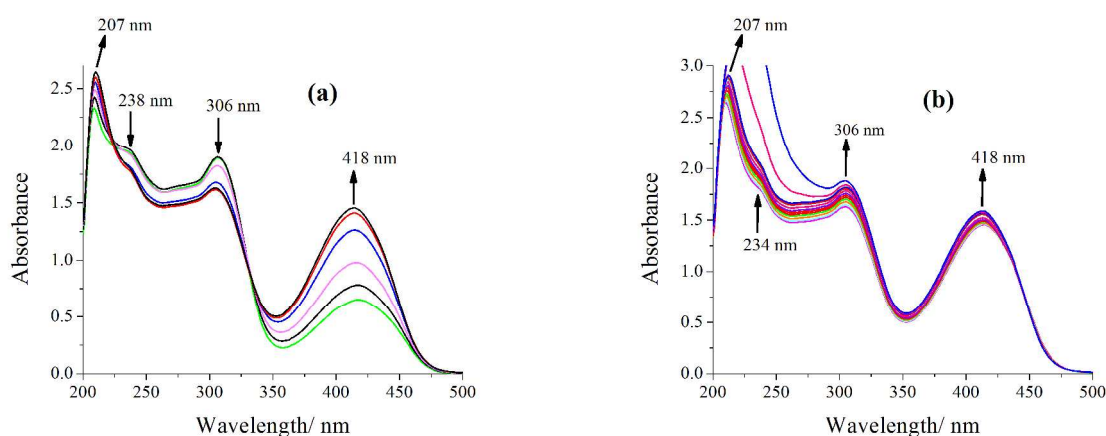


Fig. 12 Two sets (a) and (b) of spectral changes obtained during titration of stepwise additions of a H₂O₂ solution (prepared from one drop of 30 % H₂O₂ in 10 mL of MeOH) to 25 mL of ca. 6.0×10⁻⁵ M solution of [{V^VO(bzpy-tch)}₂(μ-O₂)₂] **5** in MeOH.

The ⁵¹V NMR spectra of solutions containing [V^{IV}O(acac)(bzpy-tch)] upon additions of H₂O₂ were also measured. Figure 13 depicts the change in chemical shifts of the V^V-species in solution in the presence of oxidant and upon addition of the substrate (isoeugenol). ⁵¹V NMR spectra of solutions of [{V^VO(bzpy-tch)}₂(μ-O)₂] **3** and [{V^VO(bzpy-tch)}₂(μ-O₂)₂] **5** were also measured, each showing a single resonance at -500/ -502 and -571 ppm, respectively. (Figs. S13 and S14 in the Supporting Material).

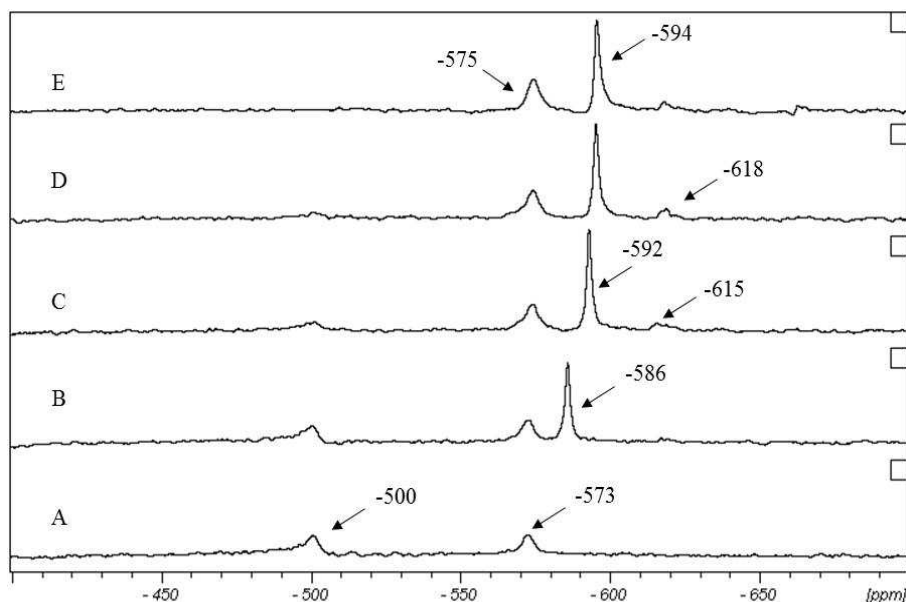


Fig. 13 ^{51}V NMR spectra of $[\text{V}^{\text{IV}}\text{O}(\text{acac})(\text{bzpy-tch})]$ (2 mM, DMF/acetone- d_6 4:1) in the presence of: A) 1 mole equivalent of H_2O_2 (0.10 M, acetone), 5 h after addition; B) 4 mole equivalents of H_2O_2 (total); C) 100 mole equivalents of H_2O_2 (total); D) 100 mole equivalents of H_2O_2 and isoeugenol; E) 48 h after the addition of 100 equivalents of isoeugenol.

The first observation is that in the presence of equimolar amounts of H_2O_2 , $[\text{V}^{\text{IV}}\text{O}(\text{acac})(\text{bzpy-tch})]$ is converted probably into $[\text{V}^{\text{V}}\text{O}_2(\text{bzpy-tch})]$, with δ_{V} at -500 ppm, and the corresponding peroxide species $[\{\text{V}^{\text{V}}\text{O}(\text{O}_2)(\text{bzpy-tch})\}]$, with $\delta_{\text{V}} = -573$ ppm. Further addition of an aqueous solution of H_2O_2 induced the appearance of another species at -586 ppm (Fig. 13B) and the decrease in the peak at -500 ppm. The species at -586 ppm, as well as those at -592 ppm (Fig. 13C), and -594 ppm (Fig. 13D, E) are probably due to $[\{\text{V}^{\text{V}}\text{O}(\text{O}_2)(\text{bzpy-tch})(\text{H}_2\text{O})\}]$, where a slow exchange (in the ^{51}V NMR time scale) between coordinated and solvated solvent molecules is taking place. This type of behavior, i.e. the detection of two distinct chemical shifts, and their change in δ_{V} upon modification of the solvent composition has been previously reported for several V^{V} -systems.^{32,33} In agreement with the possibility of obtaining suitable crystals for X-ray diffraction studies, noteworthy is the stability of the two

forms of $[\{V^V O(O_2)(bzpy-tch)(H_2O)_n\}]$ species ($n = 0, 1$), which even upon the addition of high excesses of H_2O_2 remain easily detected.

After the addition of 100 mole equivalents of oxidant, a new species appears at -618 ppm. The δ_V of $V^V O(O_2)_2$ species, in the presence of H_2O , are expected to be at more negative values than -660 ppm.^{32,34} The species at -618 ppm could be indicative of binding of HOO^- , forming either $[\{V^V O(O_2)(HOO)(Htch)\}]$ or $[\{V^V O(O_2)(HOO)(tch)\}]$, but this is only a tentative assignment,^{26,35} as this could also correspond to $V^V O(O_2)-(H_2O)_n$ species as their $51V$ NMR chemical shifts are usually also in this range.^{33,34} After addition of isoeugenol, some small modifications of the ^{51}V NMR spectra occur, but there were no clearly observable modification of the resonances at -575 , -594 and -618 ppm even after the additional 48 h period at room temperature, and another 24 h at $40^\circ C$. Again this is in agreement with the remarkable observed stability of $[\{V^V O(O_2)(bzpy-tch)\}]$, which could be easily isolated as a solid, the species at -618 ppm also remaining visible.

Reactivity of $[V^{IV} O(OMe)(bzpy-inh)]$ **2** and $[\{V^V O(bzpy-inh)\}_2(\mu-O)_2]$ **4** towards H_2O_2

The behaviour of $[V^{IV} O(OMe)(bzpy-inh)]$ **2** upon addition of H_2O_2 is entirely different from that observed for $[V^{IV} O(acac)(bzpy-tch)]$ **1**. At least four different sets of spectral changes could be identified by UV-Vis measurements upon progressive addition of H_2O_2 . Initial addition of H_2O_2 to a methanolic solution of **3** resulted in the increase of the intensity of 215, 272 and 333 nm bands without change of their λ_{max} values. For $\lambda > \sim 370$ nm the changes occurring give rise to the appearance of a shoulder band at ca. 420 nm, with the formation of two isosbestic points at 370 nm and 430 nm (Fig. 14(a)). In the next set, the λ_{max} of the 272 and 333 nm bands remain at the same positions, with only slight loss in intensity, but the 215 nm band slightly increases its intensity and the shoulder band at ca. 420 nm is converted into one at ca. 380 nm with slight increment of intensity; an isosbestic point is now formed at 365 nm (Fig. 14(b)).

Further additions of H_2O_2 cause the formation of a band at ca. 438 nm (Fig. 14(c)), along with the shift of the band at 380 nm to 390 nm. A band at 333 nm shifts to 320 nm, along with decrease of intensity. Additionally, the band at 265 nm shifts to 260 nm, along with increased intensity and the 215 nm band shifts to the red with increase of intensity.

In the fourth and last set of spectra (Fig. 14(d)), the bands at 438 and 390 nm gradually merge, with loss of intensity yielding a broad band at ca. 400 nm. The intensity of the band at 333 nm decreases continuously, while the 220 and 260 nm bands gradually merge with an increase in intensity.

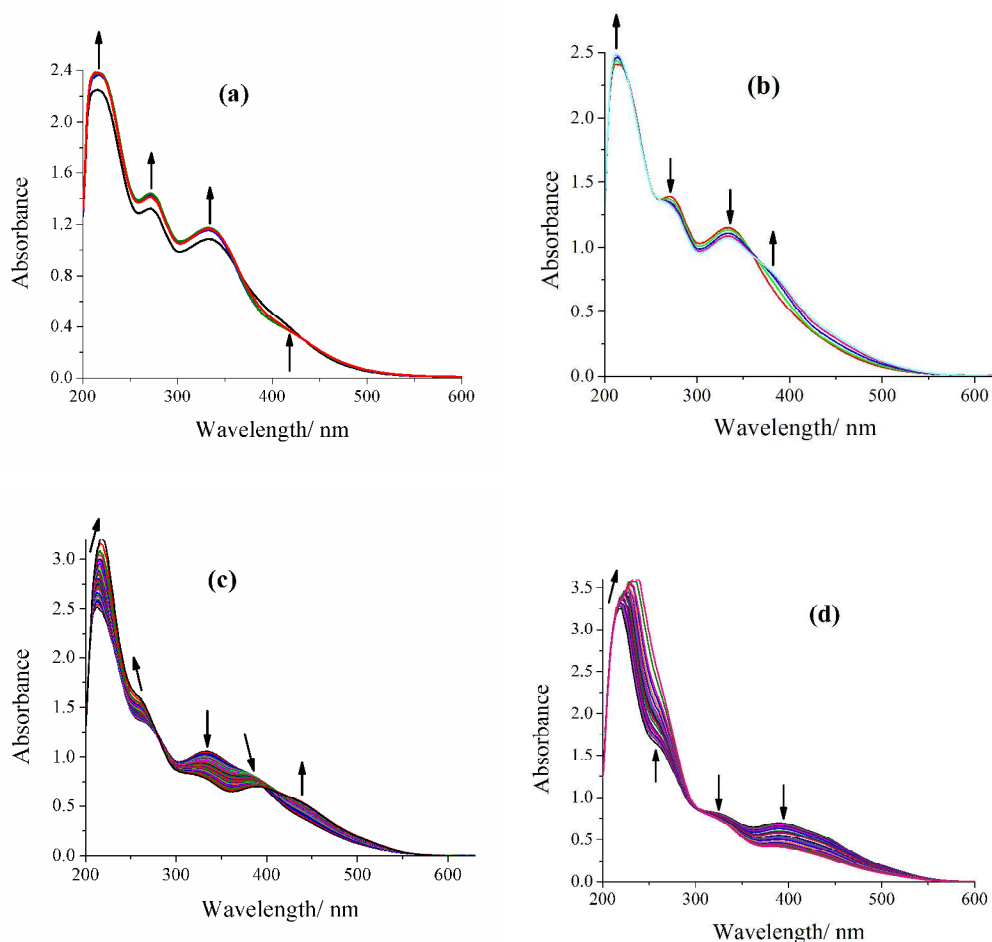


Fig. 14 Four sets (a), (b), (c) and (d) of spectral changes obtained by stepwise additions of a methanolic solution of H_2O_2 (prepared from 0.051 g (0.45 mmol) of 30 % H_2O_2 dissolved in 5 mL of MeOH) to 25 mL of ca. 9.0×10^{-5} M solution of $[\text{V}^{\text{IV}}\text{O}(\text{OMe})(\text{bzpy-inh})]$ **2** in MeOH.

Spectral changes in the d-d bands could also be observed by using solutions with higher concentration of $[\text{V}^{\text{IV}}\text{O}(\text{OMe})(\text{bzpy-inh})]$ **2**. Both bands (shoulders) at 645 and 805 nm slowly disappear upon addition of H_2O_2 (0.051 g (0.45 mmol) of 30 % H_2O_2 dissolved in 15 mL of

DMF) to **2** taken in DMF (5 mL of ca. 7.0×10^{-3} M solution in DMF) (Fig. 15). This agrees with the expected oxidation of $V^{IV}O$ -species to V^V -complexes, which in turn are converted to oxidoperoxido species upon further additions of H_2O_2 solution.

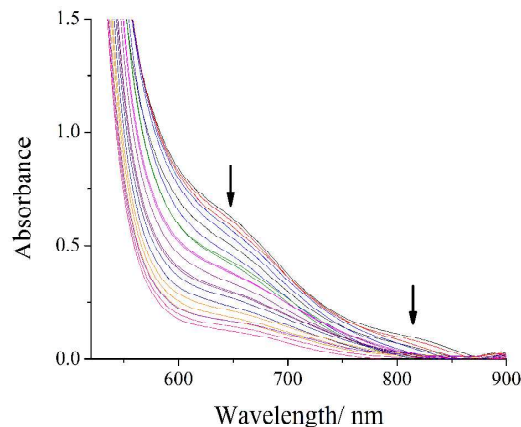


Fig. 15 Spectral changes obtained during the titration of stepwise additions of a solution (prepared from 0.051 g (0.45 mmol) of 30 % H_2O_2 dissolved in 15 mL of DMF) to 5 mL of ca. 7.0×10^{-3} M solution of $[V^{IV}O(OMe)(bzpy-inh)]$ **2** in DMF.

During the drop wise addition of a methanolic solution of H_2O_2 to a solution of $[{V^V O(bzpy-inh)}_2(\mu-O)_2]$ (**4**), the band at 396 nm slightly increases its intensity with a shift to 391 nm, while the band at 280 nm moves to 284 nm with a slight decrease in intensity (Fig. 16(a)). The band at 209 nm slightly shifts to the red with slight increase in intensity. The process generates two isosbestic points at 232 nm and 330 nm. Further additions of H_2O_2 cause the increase in intensity of the two bands (Fig. 16(b)), while the band at 284 nm shifts to higher wavelength with sharp increase in intensity.

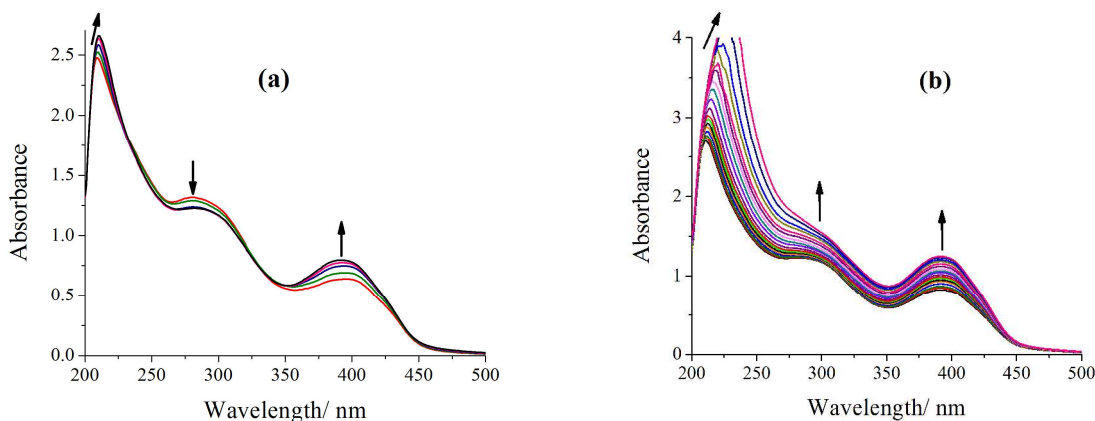


Fig. 16 Two sets of spectral changes (a) and (b) obtained by stepwise additions of a solution (prepared from 0.051 g (0.45 mmol) of 30 % H_2O_2 dissolved in 5 mL of MeOH) to 30 mL of ca. 4.8×10^{-5} M solution of $[\{\text{V}^{\text{V}}\text{O}(\text{bzpy-inh})\}_2(\mu\text{-O})_2]$ **4** in MeOH.

The ^{51}V NMR spectra of solutions of $[\{\text{V}^{\text{V}}\text{O}(\text{bzpy-inh})\}_2(\mu\text{-O})_2]$ **4** (in DMSO-d_6) and $[\{\text{V}^{\text{V}}\text{O}(\text{O}_2)(\text{bzpy-inh})\}]$ **6** (in DMF/acetone-d_6) each show a single resonance at ca. -502 and -570 ppm, respectively (Figures SI-15 and SI-16 in the SI section). The processes occurring upon addition of H_2O_2 to a solution of $[\text{V}^{\text{IV}}\text{O}(\text{OMe})(\text{bzpy-inh})]$ **2** were also monitored by ^{51}V NMR (Fig. 17).

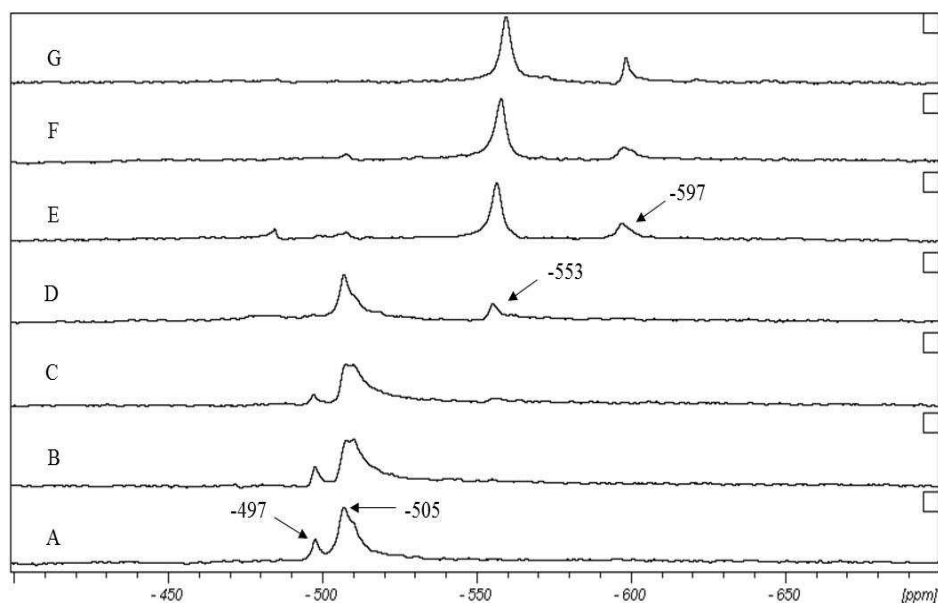


Fig. 17 ^{51}V NMR spectra of $[\text{V}^{\text{IV}}\text{O}(\text{OMe})(\text{bzpy-inh})]$ (2.0 mM, DMF/acetone- d_6 4:1) upon addition of: (A) 1.0 mole equivalent of H_2O_2 (0.10 M, acetone), 5 h after addition. (B) 2 mole equivalents of H_2O_2 (total); (C) 5 mole equivalents of H_2O_2 (total); (D) 10 mole equivalents of H_2O_2 (total); (E) 100 equivalents of H_2O_2 (total); (F) Solution of E after addition of 100 mole equivalents of isoeugenol. (G) 48 h after the addition of 100 mole equivalents of isoeugenol.

In the presence of one equivalent of H_2O_2 the solution of $[\text{V}^{\text{IV}}\text{O}(\text{OMe})(\text{bzpy-inh})]$ in DMF/acetone- d_6 4:1 is converted into $[\text{V}^{\text{V}}\text{O}_2(\text{bzpy-inh})]$ with a major signal at -505 ppm, with a shoulder at ca. -510 ppm and a minor species at -497 ppm. We tentatively assign the peak at -505 ppm and the shoulder at -510 ppm to two isomeric forms of $[\text{V}^{\text{V}}\text{O}_2(\text{bzpy-inh})(\text{H}_2\text{O})]$. The resonance at -497 ppm is assigned to $[\text{V}^{\text{V}}\text{O}_2(\text{bzpy-inh})]$, assuming that the two types of species are in slow exchange (in the ^{51}V NMR time scale) between coordinated and solvated solvent molecules, as previously reported for several V^{V} -systems.^{32,33}

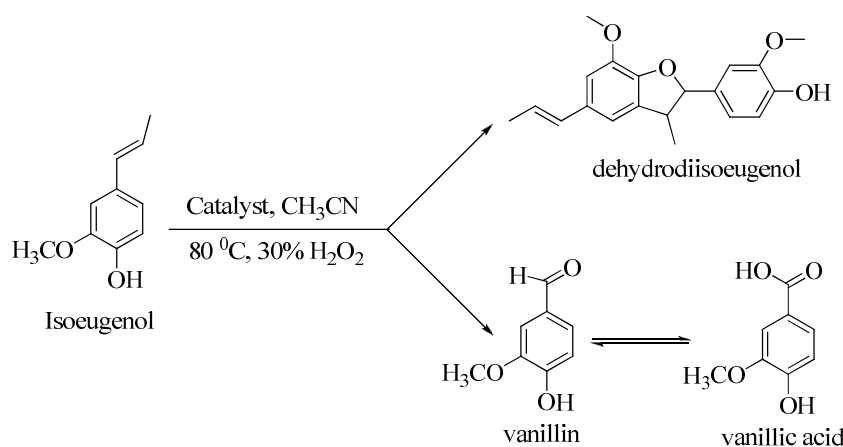
A new resonance appears at -553 ppm only after the addition of 5, but more clearly at 10 mole equivalents of H_2O_2 (spectrum D); this peak appears at -559 ppm in spectrum G. This resonance is assigned to $[\{\text{V}^{\text{V}}\text{O}(\text{O}_2)(\text{bzpy-inh})\}]$, and was observed further up field at -570 ppm upon dissolving **6** directly in DMF/acetone- d_6 4:1, thus in the absence of H_2O . Similarly to the case of **1** upon additions of a 110-fold excess of H_2O_2 solution, another species appears significantly more up field, at -597 ppm, and this could be indicative of binding of HOO^- , being tentatively assigned to either $[\text{V}^{\text{V}}\text{O}(\text{O}_2)(\text{HOO})(\text{inh})]$ or to $[\text{V}^{\text{V}}\text{O}(\text{O}_2)(\text{HOO})(\text{Hinh})]$ bearing a side-on bound hydroperoxido ligand.^{26,35} The addition of isoeugenol did not cause observable changes in the pattern of the spectrum even after an additional 48 h period at room temperature and another 24 h period at 40°C . As in the case of $[\{\text{V}^{\text{V}}\text{O}(\text{bzpy-tch})\}_2((\mu\text{-O}_2)_2)]$ **5**, this is in agreement with the observed stability of $[\{\text{V}^{\text{V}}\text{O}(\text{O}_2)(\text{bzpy-inh})\}]$, which allowed its isolation in the solid state; however, in the present case a distinct (but related) peroxide compound was characterized by single crystal X-ray diffraction analysis (see above).

Catalytic oxidation of 2-methoxy-4-(prop-1-en-1-yl)phenol (isoeugenol)

As mentioned above, vanillin is an important chemical aroma,¹² extensively used in the food industry to provide characteristic aroma and flavor of vanilla bean, quite high production

being required every year. It is mainly produced by the oxidation of isoeugenol, microbial biotransformation of isoeugenol having been the key method to produce vanillin and vanillic acid. Due to its commercial interest research to find more economic, efficient and sustainable processes for its production are required.

We have carried out the catalytic oxidation of isoeugenol using polymer supported as well as the neat V^V -complexes as catalyst precursors. We observed at least the formation of three different products namely vanillin, vanillic acid and dehydrodiisoeugenol, Scheme 4. The supported complex $PS-im[V^VO_2(bzpy-inh)]$ was used as a representative catalyst for the optimization of different reaction parameters *viz.* amounts of catalyst, oxidant (30% aqueous H_2O_2) and solvent, and temperature at which reaction was carried out while maintaining other conditions, e.g. stirring speed around 100 rpm in all reactions.



Scheme 4 Outline of the proposed scheme for the oxidation of isoeugenol, indicating the main products formed

To optimize its amount, four different amounts of catalyst (0.010, 0.020, 0.030 and 0.040 g) were taken while considering isoeugenol (0.82 g, 5.0 mmol) and other reaction parameters constant such as aqueous 30% H_2O_2 (1.13 g, 10 mmol), acetonitrile (5.0 mL) and reaction temperature ($80\text{ }^\circ\text{C}$). Information on the conversion of isoeugenol after 2 h of reaction is presented in Fig. S17. By increasing the catalyst amount from 0.010 g to 0.020 g, the conversion increased from 61 % to 89 %, but there was no further improvement in conversion on increasing it up to 0.040 g; only the amount of vanillic acid slightly increased and the relative amount of

vanillin slightly decreased. Therefore, 0.020 g of catalyst precursor was chosen as an appropriate amount for optimizing the remaining conditions.

Considering 0.020 g of catalyst precursor for 5.0 mmol of isoeugenol in 7.0 mL of acetonitrile and 80 °C reaction temperature, three different amounts of oxidant (30% H₂O₂) viz. 5.0, 10.0 and 15.0 mmol were tested. The lowest i.e. 76% conversion of isoeugenol was obtained with 5.0 mmol oxidant under above reaction conditions, whereas a maximum of 89% conversion was obtained using 10.0 mmol oxidant (product distribution: vanillic acid = 20 %, vanillin = 17 % and dehydrodiisoeugenol = 52 %); Fig. S18. Further increasing the amount of oxidant to 15.0 mmol did not improve the conversion; in fact, this decreased the formation of vanillin (product distribution: vanillic acid = 18 %, vanillin = 14 %, dehydrodiisoeugenol = 53 %). Thus, 10.0 mmol of oxidant was found suitable for the maximum conversion of isoeugenol.

The solvent (acetonitrile) also affects on the oxidation of substrate (Fig. S19). Under the above optimized reaction conditions i.e. PS-im[V^VO₂(bzpy-inh)] (0.020 g) and 30 % aqueous H₂O₂ (1.13 g, 10 mmol), three different solvent volumes i.e. 4, 7 and 10 mL for isoeugenol (0.82 g, 5.0 mmol) were taken and the reaction was carried out at 80 °C for 2 h. It was found that 4.0 mL of solvent gave the highest conversion (91 %) with product distribution: vanillic acid = 31 %, vanillin = 10 % and dehydrodiisoeugenol = 50 %. Upon increasing the solvent volume the conversion decreases as well as the % of vanillin. Thus, 4.0 mL of solvent amount was considered to be the best one for proceeding.

The effect of temperature on oxidation of isoeugenol is shown in Fig. S20. To a 5.0 mmol (0.82 g) isoeugenol in 4.0 mL of acetonitrile, PS-im[V^VO₂(bzpy-inh)] (0.020 g) and 30 % aqueous H₂O₂ (1.13 g, 10 mmol) were added and the reaction was monitored at three different temperatures viz. 60, 70 and 80 °C for 2 h. The conversion was lowest (42%) at 60 °C but improved to 84% at 70 °C. However, running the reaction at 80 °C improved this conversion to 91 %, with a product distribution of 31 % vanillic acid, 10 % vanillin and 50 % dehydrodiisoeugenol.

Details of experimental conditions and of product distribution are presented in Table 11. Thus, the optimized reaction conditions (entry no. 7) for the oxidation of 5 mmol of isoeugenol are: catalyst PS-im[V^VO₂(bzpy-inh)] (0.020 g), 30 % aqueous H₂O₂ (1.13 g, 10 mmol), acetonitrile (4 mL) and temperature 80 °C. A maximum of 18% conversion was achieved after 2

h but using 70% aqueous TBHP as oxidant under equivalent reaction conditions with a product distribution: vanillic acid = 1%, vanillin = 9% and dehydrodiisoeugenol = 8%. Blank reactions gave only ca.10 % conversion.

Details of the consumption of isoeugenol and formation of products for the catalyst precursor PS-im[V^VO₂(bzpy-inh)] are presented in Fig. 18. Under the experimental conditions presented in entry no. 7 of Table 11, the formation of all three products starts with the consumption of isoeugenol and increase with time. The formation of both vanillic acid and vanillin is poor at the beginning but vanillic acid improves considerably and reaches 30% while that of vanillin could reach only 10%. The formation of dehydrodiisoeugenol reaches 50% after 2 h of reaction time. Literature reports similar trends for the formation of these products and in all cases the overall percent formation of vanillin is low.

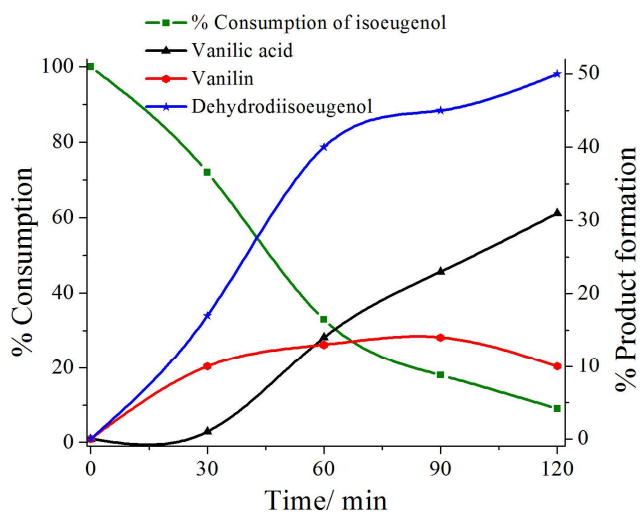


Fig. 18 Percentage consumption of isoeugenol and formation of products with time using PS-im[V^VO₂(bzpy-inh)] as catalyst precursor under the optimized conditions specified in entry 7 of Table 11.

Table 11 Results of the oxidation of 0.82 g (5.0 mmol) of isoeugenol after 2 h of reaction time using PS-im[V^VO₂(bzpy-inh)] **7** as catalyst precursor

Entry No.	Catalyst (g)	H ₂ O ₂ (g, mmol)	CH ₃ CN (mL)	Temperature (°C)	% Conv.	% product formation ^a			TOF
						VA	Vanillin	DDI	
1	0.010	1.13, 10	7	80	61	13	6	42	307
2	0.020	1.13, 10	7	80	89	20	17	52	449
3	0.030	1.13, 10	7	80	85	21	15	49	428
4	0.040	1.13, 10	7	80	86	22	14	50	433
5	0.020	0.565, 5	7	80	76	15	7	54	383
6	0.020	1.69, 15	7	80	86	18	14	53	433
7	0.020	1.13, 10	4	80	91	31	10	50	459
8	0.020	1.13, 10	10	80	84	20	9	55	423
9	0.020	1.13, 10	4	60	42	10	5	27	212
10	0.020	1.13, 10	4	70	84	26	8	50	423
11.	-	1.13, 10	4	80	10	1	8	1	-

^a VA = Vanilic acid, DDI = Dehydrodiisoeugenol

Table 12 Product selectivity and % conversion at optimum reaction conditions, chosen for maximum conversion of isoeugenol

S. No.	Catalyst	Catalyst/g	% Conv.	TOF/h ⁻¹	% product formation ^a		
					VA	Vanillin	DDI
1	PS-im[V ^V O ₂ (bzpy-tch)] 7	0.022	85	428	25	9	51
2.	PS-im[V ^V O ₂ (bzpy-inh)] 8	0.020	91	459	31	10	50
3.	PS-im[V ^V O ₂ (bzpy-tch)] 7 ^{1st cycle}	0.022	83	418	26	9	50
4.	PS-im[V ^V O ₂ (bzpy-tch)] 7 ^{2nd cycle}	0.022	80	403	25	8	51
5.	PS-im[V ^V O ₂ (bzpy-inh)] 8 ^{1st cycle}	0.020	90	454	31	9	51
6.	PS-im[V ^V O ₂ (bzpy-inh)] 8 ^{2nd cycle}	0.020	87	443	30	12	51
3.	[[V ^V O(bzpy-tch)] ₂ (μ-O) ₂] 3	1.93×10 ⁻³	70	353	19	5	46
4.	[[V ^V O(bzpy-inh)] ₂ (μ-O) ₂] 4	1.96×10 ⁻³	74	373	20	7	47

^a For abbreviations see Table 11.

In Table 12 the number of mmol of catalyst precursors taken is approximately equal in all cases, thus the catalytic activity of (**7**) and (**8**) show higher conversions (ca. 85-90% vs. 70-74%) and TON values (ca. 430-460 vs. 350-370) than their neat counterparts. The trend of formation of the different products does not differ much, but the relative amount of dehydrodiisoeugenol formed is higher in the cases of (**3**) and (**4**). Additionally, the recycle ability of the polymer-supported complexes (see Table 12) makes them even better catalysts over the non polymer-supported ones for the production of vanillin and vanilic acid. The vanadium contents obtained after first catalytic use of catalysts **7** and **8** are 0.219 and 0.198 mmol g⁻¹ of resin, respectively which also indicate that the leaching of polymer-supported complexes is in very small amount.

Conclusions

Upon reaction of Hbzpy-tch **I** and Hbzpy-inh **II** with [V^{IV}O(acac)₂] in dry methanol two different types of V^{IV}O-complexes were obtained and characterized: [V^{IV}O(acac)(bzpy-tch)] **1** and [V^{IV}O(OMe)(bzpy-inh)] **2**, respectively. Compound **2**, containing coordinated MeO⁻, corresponds to a rather unusual formulation for a V^{IV}O-compound, where MeO⁻ is one of the ligands; the measured EPR spectrum in solution agrees with the equatorial binding of MeO⁻ to V^{IV}. Upon oxidation in methanolic solution, the corresponding monomeric V^VO₂-complexes are probably obtained in solution, but irrespective of their nature in methanol in the solid state both types of compounds yielded dinuclear [{V^VO(bzpy-tch)}₂(μ-O₂)] **3** and [{V^VO(bzpy-inh)}₂(μ-O₂)] **4** which were characterized by single-crystal X-ray diffraction. These V^V-compounds can also be prepared directly in methanol by reacting [V^{IV}O(acac)₂] with the ligands followed by aerial oxidation.

Treatment of **1** or **2** in methanol with H₂O₂ yielded the corresponding [V^VO(O₂)(L)] complexes, probably [V^VO(O₂)(bzpy-tch)] and [V^VO(O₂)(bzpy-inh)] in solution, which upon isolation in the solid state and the corresponding single-crystal X-ray diffraction analysis confirmed the formation of [{V^VO(O₂)(bzpy-tch)}₂μ-O₂] **5** and [V^VO(O₂)(bzpy-inh)(H₂O)]·0.5MeOH **6a**. Compound **6a** corresponds to a quite unusual structure for a V^V-peroxido complex. This complex corresponds to a dinuclear species containing two V^V-centers. Each V^V adopts a distorted seven-coordinated pentagonal bipyramidal geometry which includes two peroxido ligands that also act as monodentate bridges between the two V^V-centers.

Globally the spectroscopic studies in solution, upon making stepwise additions of H₂O₂ solution to the V^{IV}-precursors, were explained by their oxidation to V^V-species followed by the formation of the corresponding V^VO(O₂)(L) complexes. Upon standing for several days in the presence of a large excess of H₂O₂, followed by addition of equivalent amounts of substrate, the corresponding ⁵¹V NMR peaks continued being clearly detected. This indicates an unusual and remarkable stability of the V^V-peroxido complexes **5** and **6**.

Reaction of **3** and **4** with PS-im in DMF gave PS-im[V^VO₂(bzpy-inh)(MeOH)] **7** and PS-im[V^VO₂(bzpy-tch)(MeOH)] **8**, and these polymer-grafted compounds were used for the catalytic oxidation of isoeugenol. The catalytic activity of **7** and **8** showed higher conversions (ca. 85-90% vs. 70-74%) and TON values (ca. 430-460 vs. 350-370) than their neat counterparts. These could be recycled and re-used with small loss of activity upon each cycle. The recycle ability of the grafted complexes gives **7** and **8** additional advantages over the corresponding neat ones for the catalytic oxidation of isoeugenol.

Electronic supplementary information available:

Table S1 (Spin Hamiltonian parameters corresponding to the V^{IV}-impurities present in the initial samples of **4**, **7** and **8**), Figs. S1-S4 (¹H NMR), Figs. S5-S8 (¹³C NMR), S9-S11 (ESI-Mass), Fig. S12 (EPR) and Figs. S13-S16 (⁵¹V NMR) and oxidation of isoeugenol under various reaction conditions (Figs. S17-S20). CCDC 1018367 (**3**) 1018368 (**4**), 1018365 (**5**) and 1018366 (**6a**). For ESI and crystallographic data in CIF or other electronic format see DOI: xxxxxxxx.

Acknowledgments

MRM thank the Department of Science and Technology, the Government of India, New Delhi for financial support of the work (SR/S1/IC-32/2010). NC acknowledge Council of Scientific and Industrial Research, New Delhi for fellowship. This work was supported by Fundação para a Ciência e a Tecnologia (FCT), PEst-OE/QUI/UI0100/2013, the IST-UTL Centers of the Portuguese NMR and Mass Spectrometry Networks (REM2013, RNNMR), RECI/QEQ-QIN/0189/2012, RECI/QEQ-MED/0330/2012, grant SFRH/BPD/79778/2011 and the Investigator FCT programme.

References

1. (a) D. C. Crans, A. D. Keramidas, S. S. Amin, O. P. Anderson and S. M. Miller, *J. Chem. Soc., Dalton Trans.*, 1997, 2799–2812; (b) M. R. Maurya, S. Khurana, W. Zhang, D. Rehder, *J. Chem. Soc., Dalton Trans.*, 2002, 3015–3023.
2. (a) M. R. Maurya, A. Kumar, M. Ebel and D. Rehder, *Inorg. Chem.*, 2006, **45**, 5924–5937; (b) M. R. Maurya, A. Arya, A. Kumar, M. L. Kuznetsov, F. Avecilla, J. Costa Pessoa, *Inorg. Chem.*, **49** (2010) 6586–6600.
3. (a) M. R. Maurya, S. Agarwal, M. Abid, A. Azam C. Bader, M. Ebel and D. Rehder, *Dalton Trans.*, 2006, 937–947; (b) M. R. Maurya, N. Chaudhary and F. Avecilla, *Polyhedron*, 2014, **67**, 436–448; (c) M. R. Maurya, N. Chaudhary, A. Kumar, F. Avecilla and J. Costa Pessoa, *Inorg. Chim. Acta*, 2014, **420**, 24–38.
4. (a) M. R. Maurya, A. Arya, A. Kumar and J. Costa Pessoa, *Dalton trans.*, 2009, 2185–2195; (b) M. R. Maurya, A. Arya, U. Kumar, A. Kumar, F. Avecilla and J. Costa Pessoa, *Dalton Trans.*, 2009, 9555–9566; (c) M. R. Maurya, M. Bisht, A. Kumar, M. L. Kuznetsov, F. Avecilla and J. Costa Pessoa, *Dalton Trans.*, 2011, **40**, 6968–6983; (d) M. R. Maurya, M. Bisht and F. Avecilla, *J. Mol. Catal. A: Chem.*, 2011, **344**, 18–27; (e) M. R. Maurya, M. Bisht and F. Avecilla, *Indian J. Chem.*, 2011, **50A**, 1492–1503.
5. (a) X. Li, M. S. Lah and V. L. Pecoraro, *Inorg. Chem.*, 1988, **27**, 4657–4664; (b) L. M. Mokry and C. J. Carrano, *Inorg. Chem.*, 1993, **32**, 6119–6121; (c) G. Asgedom, A. Sreedhara, J. Kivikoski, E. Kolehmainen and C. P. Rao, *J. Chem. Soc., Dalton Trans.*, 1996, 93–97; (d) S. N. Pal and S. Pal, *J. Chem. Crystalogr.*, 2000, **30**, 329; (e) V. D. Defflon, D. M. de Oliveira, G. F. de Sousa, A. A. Batista, L. R. Dinelli and E. E. Castellano, *Z. Anorg. Allg. Chem.*, 2002, **628**, 1140–1144.
6. M. R. Maurya, S. Khurana, W. Zhang and D. Rehder, *Eur. J. Inorg. Chem.*, 2002, 1749–1760.
7. M. R. Maurya, M. Kumar and A. Arya, *Catal. Commun.*, 2008, **10**, 187–191.
8. (a) G. Grivani, S. Tangestaninejad, M. H. Habibi, V. Mirkhani and M. Moghadam, *Appl. Catal. A: Gen.*, 2006, **299**, 131–136; (b) S. Tangestaninejad, M. H. Habibi, V. Mirkhani and G. Grivani, *J. Mol. Catal. A: Chem.*, 2006, **255**, 249–253.
9. (a) M. R. Maurya and J. Costa Pessoa, *J. Organometal. Chem.*, 2011, **696**, 244–254; (b) M. R. Maurya, A. Kumar and J. Costa Pessoa, *Coord. Chem. Rev.*, 2011, **255**, 2315–2344.
10. J. Costa Pessoa, I. Correia, P. Adão, in *Advances in Organometallic Chemistry and Catalysis*, ed. A. J. L. Pombeiro, John Wiley & Sons, Chapter 17, 2014, pp. 227–232.
11. L. Zheng, P. Zheng, Z. Sun, Y. Bai, J. Wang and X. Guo., *Bioresour. Technol.*, 2007, **98**, 1115–1119.

12. R. Seshadri, A. S. Lamm, A. Khare and J. P. N. Rosazza, *Enzyme Microb. Technol.*, 2008, **43**, 486–494.
13. D. Hua, C. Ma, S. Lin, L. Song, Z. Deng, Z. Maomy, Z. Zhang, B. Yu and P. Xu, *J. Biotechnology*, 2007, **130**, 463–470.
14. (a) K. Li and J. W. Frost, *J. Am. Chem. Soc.*, 1998, **120**, 10545–10546; (b) P. Venkitasubramanian, L. Daniels, S. Das, A. S. Lamm and J. P. N. Rosazza, *Enzyme Microb. Technol.*, 2008, **42**, 130–137; (c) T. Li and J. P. N. Rosazza, *Appl. Environ. Microbiol.*, 2000, **66**, 684–687; (d) H. Priefert, J. Rabenhorst and A. Steinbüchel, *Appl. Microbiol. Biotechnol.*, 2001, **56**, 296–314.
15. V. Augugliaro, G. Camera-Roda, V. Loddo, G. Palmisano, L. Palmisano, F. Parrino and M. A. Puma, *Appl. Catal. B: Environ.*, 2012, **111–112**, 555–561.
16. E. V. Gusevskaya, L. Menini, L. A. Parreira, R. A. Mesquita, Y. N. Kozlov and G. B. Shul'pin, *J. Mol. Catal. A: Chem.*, 2012, **363–364**, 140–147.
17. M. Kuriakose, M. R. P. Kurup and E. Suresh, *Polyhedron*, 2007, **26**, 2713–2718.
18. R. A. Rowe and M. M. Jones, *Inorg. Synth.*, 1957, **5**, 113–116.
19. M. Kuriakose, M. R. P. Kurup and E. Suresh, *Spectrochim. Acta A*, 2007, **66**, 353–358.
20. G. M. Sheldrick, SHELXL-97: An Integrated System for Solving and Refining Crystal Structures from Diffraction Data (Revision 5.1); University of Göttingen, Germany, 1997.
21. (a) A. S. Ogunlaja, W. Chidawanyika, E. Antunes, M. A. Fernandes, T. Nyokong, N. Torto and Z. R. Tshentu, *Dalton Trans.*, 2012, **41**, 13908–13918; (b) R. S. Walmsley, A. S. Ogunlaja, M. J. Coombes, W. Chidawanyika, C. Litwinski, N. Torto, T. Nyokong and Z. R. Tshentu, *J. Mater. Chem.*, 2012, **22**, 5792–5800; (c) Z. R. Tshentu, C. Togo and R. S. Walmsley, *J. Mol. Catal. A: Chem.*, 2010, **318**, 30–35.
22. (a) I. Correia, J. Costa Pessoa, M. T. Duarte, R. T. Henriques, M. F. M. da Piedade, L. F. Veiros, T. Jakusch, T. Kiss, I. Dornyei, M. M. C. A. Castro, C. F. G. C. Geraldes and F. Avecilla, *Chem. Eur. J.*, 2004, **10**, 2301–2317; (b) P. Adão, M. R. Maurya, U. Kumar, F. Avecilla, R. T. Henriques, M. L. Kusnetsov, J. Cost Pessoa, and I. Correia, *Pure Appl. Chem.*, 2009, **81**, 1279–1296.
23. W. Plass, *Angew. Chem., Int. Ed. Engl.*, 1996, **35**, 627–631.
24. F. Avecilla, P. Adão, I. Correia and J. Costa Pessoa, *Pure Appl. Chem.*, 2009, **81**, 1297–1311.

25. C. Gabriel, E. Kioseoglou, J. Venetis, V. Psycharis, C. P. Raptopoulou, A. Terzis, G. Voyiatzis, M. Bertmer, C. Mateescu and A. Salifoglou, *Inorg. Chem.*, 2012, **51**, 6056–6069.
26. M. R. Maurya, C. Haldar, A. Kumar, M. Kuznetsov, F. Avecilla and J. Costa Pessoa, *Dalton Trans.*, 2013, **42**, 11941–11962.
27. (a) A. D. Westland, F. Haque and J.-M. Bouchard, *Inorg. Chem.*, 1980, **19**, 2255; (b) K. Nakamoto, *Infrared and Raman Spectra of Inorganic Compounds, Part B: Applications in Coordination, Organometallic, and Bioinorganic Chemistry*, 5th edn, John Wiley & Sons, New York, 1997.
28. A. Rockenbauer and L. Korecz, *Appl. Magn. Reson.*, 1996, **10**, 29–43.
29. (a) K. Wüthrich, *Helv. Chim. Acta*, 1965, **48**, 1012–1017. (b) N. D. Chasteen, in: J. Reuben (Ed.), “Biological Magnetic Resonance”, Plenum, New York, p. 53 (1981).
30. T. S. Smith, R. Lobrutto and V. L. Pecoraro, *Coord. Chem. Rev.*, 2002, **228**, 1–18.
31. E. Garribba, G. Micera and D. Sanna, *Inorg. Chim. Acta*, 2006, **359**, 4470–4476.
32. V. Conte, F. Furia and S. Moro, *Inorg. Chim. Acta*, 1998, **272**, 62–67.
33. (a) C. T. Miranda, S. Carvalho, R. T. Yamaki, E. B. Paniago, R. H. U. Borges and V. M. De Bellis, *Polyhedron*, 2010, **29**, 897–903; (b) I. Andersson, A. Gorzas and L. Pettersson, *Dalton Trans.*, 2004, 421–428; (c) H. Faneca, V. A. Figueiredo, A. I. Tomaz, G. Gonalves, F. Avecilla, M. C. Pedroso de Lima, C. F. G. C-Geraldes, J. Costa Pessoa and M. M. C. A. Castro, *J. Inorg. Biochem.* 2009, **103**, 601–608.
34. (a) V. Conte, F. Furia and S. Moro, *Inorg. Chim. Acta*, 1998, **272**, 62–67; (b) Pettersson, *Coord. Chem. Rev.*, 2003, **237**, 77–87.
35. (a) D. Balcells, F. Maseras, G. Ujaque, *J. Am. Chem. Soc.* 2005, **127**, 3624–3634; (b) J. Y. Kravitz, V. L. Pecoraro, H. A. Carlson, *J. Chem. Theory Comput.* 2005, **1**, 1265–1274; (c) C. J. Schneider, J. E. Penner-Hanh, V. L. Pecoraro, *J. Am. Chem. Soc.* 2008, **130**, 2712–2713.

Table of Contents Synopsis

Oxidovanadium(IV) and dioxidovanadium(V) complexes of hydrazones of 2-benzoylpyridine and their catalytic applications

M.R. Maurya, N. Chaudhary, F. Avecilla, P. Adão, and J. Costa Pessoa

V^V -polymer-supported compounds, their neat analogues and corresponding peroxido-complexes are prepared and applied as catalyst precursors for the oxidation of isoeugenol.

